# Multimodal Profiling of Repair-Associated Immune Dynamics in a Mouse Model of Menstruation

Rebecca J. Ainslie[1,2], Phoebe M. Kirkwood[1], Hanning Li[1], Symeon Gerasimou[1], Philippa T.K. Saunders[1], Ioannis Simitsidellis[1], and Douglas A. Gibson[1,2*]

*[1]Centre for Reproductive Health and [2]Centre for Inflammation Research, Institute for Regeneration and Repair, University of Edinburgh, Edinburgh BioQuarter, 4-5 Little France Crescent, Edinburgh EH16 4UU.*

[*]Corresponding Author

Douglas Gibson, Principal Investigator & Sir Henry Dale Fellow

Institute for Regeneration and Repair

The University of Edinburgh

Edinburgh BioQuarter

4-5 Little France Drive

Edinburgh

EH16 4UU

E-mail: D.A.Gibson@ed.ac.uk

Abstract

Despite the importance of inflammation to menstruation, we lack detailed understanding of how immune dynamics contribute to endometrial repair. We performed detailed phenotypic characterisation of uterine immune cells using single cell RNA sequencing, flow cytometry and multiplex immunohistochemistry in a mouse model of simulated menstruation. Uterine tissues were collected from age-matched controls or from key phases of menstruation, including tissue breakdown, repair and remodelling. Our findings reveal distinct compositional changes across different phases of menstruation and highlight predominant roles for monocytes, macrophages, and neutrophils in endometrial repair. Immunohistochemistry revealed the spatial association of these myeloid cell subsets with areas of tissue repair and remodelling. Bioinformatic analysis highlighted key roles for monocyte, macrophage and neutrophil signalling during endometrial repair with thrombospondin 1 and secreted phosphoprotein 1 emerging as key signalling pathways. These data significantly advance our understanding of menstrual physiology and identify potential therapeutic targets for menstrual disorders.

31 **40-word summary:**

32 This study investigates immune cell dynamics in a mouse model of menstruation, highlighting
33 roles for monocytes, macrophages, and neutrophils in non-fibrotic endometrial repair, and
34 identifies key signalling pathways as potential therapeutic targets for menstrual disorders.

## Introduction

Menstruation is characterised by an inflammatory cascade resulting in the breakdown and shedding of the functional layer of the endometrium followed by phases of endometrial repair and remodelling [1-4].This extensive inflammatory process must be tightly regulated to maintain reproductive function, with deficits in endometrial repair associated with reproductive health disorders [5]. Despite the importance of inflammation to menstruation and reproductive health, our current understanding of how inflammatory cells contribute to endometrial repair is limited.

Studies investigating endometrial immune cell composition during human menstruation have relied on immunohistochemistry analysis of fixed tissues with limited direct profiling of immune cell subsets. These studies have reported that the abundance of monocytes and macrophages dramatically increase prior to menstruation [6] whilst neutrophils are increased during endometrial breakdown and repair [7, 8]. Profiling of lymphoid cells is more limited. A study in the 1990's suggested CD8+ T cells are increased post-menstruation during the early-mid proliferative phase of the cycle [9]. B cells are sparse in the endometrium throughout the cycle and therefore their role during menstruation has not been investigated [10]. In contrast, while uterine natural killer cells (uNKs) are abundant in the late secretory phase and in association with fertility regulation, their numbers are reportedly low during menstruation [11, 12] suggesting they may not play a significant role in endometrial repair.

The generation of human scRNAseq datasets have increased our understanding of the composition of endometrial immune cells in the proliferative and secretory phases of the menstrual cycle [13, 14]. However, studies profiling immune cells in tissue samples from the menstrual phase are lacking. To overcome these limitations we, and others, have developed and validated a refined mouse model of simulated menstruation [15] to gain insights into tissue dynamics, immune cell composition and mechanisms of scarless repair. Although mice don't naturally menstruate, the physiological changes that occur in the human endometrium can be modelled using hormonal priming and artificial stimulation of implantation. Following hormone

withdrawal, uterine tissues undergo reproducible breakdown and repair, recapitulating key features of human menstruation including rapid re-epithelialisation, stromal cell remodelling and endothelial cell proliferation [15].

We have previously used this mouse model of menstruation to investigate the role of uterine macrophages during endometrial repair which identified distinct monocyte and macrophage populations with spatially discrete distributions[16]. Specifically, immunohistochemistry analysis revealed that monocyte-derived macrophages were located in areas of the endometrium actively undergoing repair whilst tissue-resident macrophages were restricted to areas that have previously undergone repair [16]. Macrophages have been shown to contribute to endometrial shedding through the production of matrix metalloproteinases that degrade the extracellular matrix and through the production of vascular endothelial growth factor [17, 18]. Neutrophils are abundant during menstruation and are associated with apoptosis and cytokine production but whether they contribute to endometrial repair has not been explored [7, 8]. Cytokines and growth factors that support tissue breakdown and repair include pro-inflammatory cytokines (IL-1$\beta$, TNF-$\alpha$, IL-6)[19, 20], chemokines (CCL2, CCL5, CXCL8) [8, 21] and regulators of matrix degradation and remodelling (MIF, MMPs, prostaglandins, VEGF) [1, 22, 23]. However, expression of these mediators has mostly been reported in whole tissues, limiting interpretation of cell-specific factors. Although immune cell types and mediators in menstruation have been profiled to some extent, deeper phenotyping of endometrial repair processes is needed to advance our understanding of menstrual physiology.

Menstruation is a complex and dynamic inflammatory process, but the contribution of distinct immune cell subsets and mediators remains poorly understood. To address this, we performed detailed phenotypic characterisation of uterine immune cells in a mouse model of simulated menstruation scRNAseq, flow cytometry and multiplex immunohistochemistry. We describe temporal and spatial association of myeloid cells with regions of tissue repair and highlight putative repair-associated signalling pathways associated with these cell types. Collectively,

89 these data provide new insights into inflammatory regulation of menstruation and identify key
90 pathways could be future therapeutic targets in menstrual disorders.

91 Materials and Methods

92 *Mouse model of simulated menstruation*

93 All animal work was carried out according to best practise in line with the Animal Welfare and
94 Ethical Review Body (AWERB) and under licensed approval from the UK Home Office. The
95 mouse model of simulated menstruation was conducted in accordance with standard protocols
96 that have been described in detail in previous studies[8, 15, 16, 24, 25]. Briefly, female mice
97 between eight to ten weeks of age underwent dorsal bilateral ovariectomy (d0) and were given
98 daily injections of 17β-oestradiol (E2) in sesame oil (100ng/100µl, d7-9). A progesterone (P4)-
99 secreting pellet was inserted subcutaneously on d13; mice also received daily injections of E2
100 (5ng/100µl; d13-15). On d15, decidualisation was induced by trans-cervical introduction of
101 sesame oil into the uterine lumen (40µl, d15). Removal of the P4 pellet (d19) results in a rapid
102 decline in progesterone, stimulating the breakdown and shedding of the decidual mass which
103 simulates human menstruation in the mouse. Uterine tissues were collected at various time
104 points following progesterone withdrawal (0-, 12-, 24-, and 48 hr) as well as from age-matched
105 mice (~3-month-old, oestrus cycling). A schematic of the mouse model of simulated
106 menstruation and gross morphological changes that occur in the endometrium during phases
107 of tissue breakdown, repair and remodelling can be seen in figure S1.

108 *Bioinformatics analysis of single cell RNA sequencing data:*

109 ScRNAseq analysis was performed on total leukocytes ($CD45^+$ live singlets) isolated from
110 uterine tissues 24- (n=4) and 48 hrs (n=4) following progesterone withdrawal, representing
111 time points of endometrial tissue repair and remodelling respectively, and compared to age-
112 matched cycling/control tissues (n=8). $CD45^+$ cells were recovered using fluorescence-
113 activated cell sorting (FACS), pooling 25,000 cells per sample to give a total of 100,000 cells
114 for input to the 24/48hr dataset and 200,000 cells for input to the cycling dataset. Isolated cell
115 suspensions were counted, and viability confirmed to be >85% using a TC20 Automated Cell
116 Counter (BioRad, Cat. No. 1450102). Cell suspensions were processed using the 10x
117 Chromium Controller (10x Genomics, USA) to partition single cells into Gel bead-in-Emulsions

118 (GEMs) containing unique 10x barcodes and cDNA libraries generated following standard
119 protocol
120 ls as previously described[24, 25]. Sequencing was carried out on the Illumina NovaSeq
121 platform using bespoke 10x parameters, according to standard protocols (Edinburgh
122 Genomics: http://genomics.ed.ac.uk/, Edinburgh).

123 Raw data files were processed using 10x Cell Ranger (version 2.0.1,
124 https://www.10xgenomics.com) and downstream QC, clustering and gene expression analysis
125 performed in *Seurat [26]* (Version 3) following analysis pipelines described previously[24, 25].
126 Data were filtered based on standard QC metrics: number of unique genes detected in each
127 cell (nFeature_RNA >200 & <5000); the percentage of mitochondrial genes (<10%); and the
128 percentage ribosomal genes (<10%). The Scrublet python package was used to further
129 identify and remove putative doublets from scRNAseq data[27]. Individual datasets were
130 combined using Seurat's 'anchor-based' integration workflow to facilitate accurate
131 comparative analysis between experimental conditions. Following integration, data were
132 normalised and scaled prior to unsupervised clustering based on PCA analysis of the most
133 variably expressed genes using a graph-based approach ('FindNeighbours', 'FindClusters). A
134 quantitative method was used alongside the 'ElbowPlot' function to determine the number of
135 principle components required to capture the majority of the variance in the data[28]. Resultant
136 clusters were visualised using the uniform manifold approximation and projection (UMAP)
137 method and differential gene expression analysis was performed ('FindAllMarkers') to identify
138 cluster specific gene signatures using the non-parametric Wilcoxon rank sum test and p-value
139 threshold of <0.05. Over-represented functional annotations associated with the differentially
140 expressed genes (DEGs) were detected using the clusterProfiler package[29] using core
141 functions to interpret data in the context of biological function, pathways, and networks.

142 The R package CellChat [30] (version 2) was utilised to investigate cellular interactions
143 between immune cell types. CellChat estimates the probability of cell-cell communication via

144 the integration of single cell gene expression data with a database (CellChatDB) of known
145 signalling ligands and receptors generated from the literature.

146 The data discussed in this study will be deposited in NCBI's Gene Expression Omnibus on
147 publication [31].

148 *Flow cytometry:*

149 Uterine tissue samples were dissected and transferred to PBS kept at 4°C prior to the tissue
150 digestion protocol. Individual uterine horns were analysed as distinct samples given the
151 potential for each to exhibit varying degrees of decidualisation in response to the
152 stimulus. Tissue processing for flow cytometry analysis was performed as described
153 previously [24, 25]. Briefly, uterine tissues were manually dissociated and incubated with
154 collagenase (1mg/ml) and DNase (0.1mg/ml) for 30 min at 37°C. Tissues were further
155 dispersed and washed in FACS buffer (PBS Ca2-Mg2-: 5% charcoal stripped foetal calf serum
156 (CSFCS – Cat. No. 12676029), 2mM EDTA) and subsequently strained through 70µm and
157 40µm cell strainers. Cell suspensions were centrifuged at 400rcf for 5 min and cell pellets re-
158 suspended in 1ml ACK lysing buffer (Gibco, Cat. No. A10492-01) for 1 min then washed.
159 Uterine cell suspensions were incubated with LIVE/DEAD Red (Life Technologies Ltd,
160 L34971) for 30 min on ice followed by incubation with Mouse TruStain FcXTM (Biolegend
161 101319; 1:1000) for 10 min on ice. Cell suspensions were subsequently incubated with
162 optimised dilutions of fluorescently conjugated extracellular antibodies for 30 min on ice, as
163 detailed in Table 1 –- Figure 2.

164 Following antibody incubation, single cell suspensions were washed and re-suspended in
165 FACS buffer at 4°C and analysed using a Cytek Aurora (Cytek Biosciences) and SpectroFlo
166 software. Data analysis was performed using FlowJo analysis software (FlowJo LLC, Oregon,
167 USA).

168 *Tissue recovery, processing and Haematoxylin and Eosin staining*

169 Mouse uteri were fixed in 10% neutral buffered formalin for 24 hr at 4°C before transfer into
170 70% ethanol, at which point they could be stored long term. Tissues were then processed
171 according to standard protocols for paraffin embedding by the University of Edinburgh
172 Histology Facility. Sections from formalin-fixed paraffin-embedded (FFPE) blocks were cut at
173 5um thickness using a microtome and the sections were placed on Xtra adhesive pre-cleaned
174 micro slides (Surgipath, Leica Biosystems) and placed in at 60°C for 15 min prior to staining.

175 For visualisation of tissue morphology, staining was performed with haematoxylin and eosin.

176 *Immunohistochemistry and Immunofluorescence*

177 For immunohistochemistry and immunofluorescence, FFPE uterine sections of 5um thickness
178 were deparaffinised and rehydrated using a series of xylene and alcohols followed by antigen
179 retrieval in Citrate retrieval buffer (pH6) for 5 min in an Instant Pot. Following washes with tap
180 water, the sections were incubated with 3% (v/v) hydrogen peroxide solution in PBS for 30
181 min at room temperature, followed by several blocking steps with serum from the species the
182 secondary antibody was raised in, to avoid nonspecific binding of antibodies. Sections were
183 incubated with the primary antibody diluted in serum blocking solution overnight at 4°C.
184 Negative controls were included, in which the primary antibody was omitted to identify any
185 nonspecific binding by the secondary antibody. Primary antibodies against CD3 (1:250
186 dilution; NB600-1441, Novus Biologicals), B220 (1:250 dilution; 14-0452-82, Invitrogen), CD14
187 (1:6000 dilution; ab221678, Abcam), CD64 (1:6000 dilution; 50086-R008, Sino Biological),
188 Ly6G (1:10000 dilution; 127649, Biolegend) and DBA-lectin (1:1000 dilution; B-1035, Vector)
189 were used in this study.

190 The following day, sections were washed with 0.05% Tween in PBS followed by an incubation
191 with an HRP-conjugated secondary antibody (1:500 dilution) in serum blocking solution for 30
192 min at room temperature followed by an incubation with either DAB substrate for 5 min at room
193 temperature (ab64238, Abcam) or Opal Polaris solution (FP1487001KT [Opal 520],
194 FP1488001KT [Opal 570], FP1496001KT [Opal 650], Akoya Biosciences) for 10 min at room
195 temperature. After staining, sections were washed and counterstained either with

196 Haematoxylin or DAPI (1:3000 dilution; 10236276001, Sigma-Aldrich). For chromogenic
197 immunohistochemistry, the sections were dehydrated in a series of alcohols and mounted on
198 coverslips with Pertex mounting medium (SEA-0100-00A, CellPath), while for
199 immunofluorescence, the sections were mounted on coverslips with Fluoromount (0100-01,
200 Cambridge Bioscience). Slides were imaged with a slide scanner (Axioscan 7, Zeiss) or an
201 inverted microscope (Axio Observer, Zeiss) and images were exported using the Zen 3.9
202 software (Zeiss).

203 *Statistical analysis*

204 Statistical analysis was performed using Graphpad prism software (version 10). Brown-
205 Forsythe and Welch tests were used to determine significance between experimental
206 conditions in data that were normally distributed. Non-parametric testing was utilised where
207 sample sizes were insufficient to confirm normality of data distribution or where the data was
208 not normally distributed; Kruskal-Wallis tests were used to assess differences between
209 experimental conditions. All data are presented as mean ± SD and criteria for significance is
210 $p<0.05$.

211 Results

212 *Single-cell RNA sequencing identifies distinct immune cell populations in the mouse uterus*
213 *associated with endometrial tissue repair and remodelling.*

214 To investigate the phenotype and function of immune cells during endometrial repair, single
215 cell RNA sequencing (scRNAseq) analysis was performed on $CD45^+$ immune cells isolated
216 from uterine tissues recovered at key time points of an established mouse model of
217 menstruation: 24- and 48 hr post progesterone withdrawal and in age-matched controls
218 ('cycling') (figure S1). These timepoints are representative of active tissue repair (24 hr,
219 'repair') and tissue remodelling (48 hr, 'remodelling'). Following quality control and filtering of
220 sequencing data, 13,498 $CD45^+$ immune cells were detected across 3 experimental conditions
221 (cycling: 5,379 cells; repair: 3,761 cells; and remodelling: 4,358 cells) and integrated for

222 downstream analysis. Unsupervised clustering resulted in the identification of 8
223 transcriptionally distinct clusters of immune cells in uterine tissues: neutrophils, eosinophils,
224 monocytes, macrophages, dendritic cells, NK cells, T cells and B cells (Figure 1A). Cell
225 clusters were annotated using both the expression of established immune cell gene markers
226 (Figure 1B) and analysis of the top 10 most differentially expressed genes (DEGs) per cluster
227 (Figure 1C & 1D).

228 Analysis of immune cell clusters relative to experimental condition identified distinct changes
229 in immune cell composition during endometrial repair and remodelling. Innate immune
230 populations including neutrophils, monocytes and to a lesser degree macrophages, dendritic
231 cells and eosinophils were predominant in the 'repair' dataset, while adaptive immune
232 populations such as T, B and NK cells, were largely only present in the 'cycling' and
233 'remodelling' data (Figure 1E & 1F). Relative abundance analysis within each experimental
234 condition showed changes in uterine immune cell composition in response to endometrial
235 repair (Figure 1G). Most notable was an increase in the proportion of neutrophils and
236 monocytes during active endometrial repair (24-hour) which remained elevated during the
237 remodelling phase (48-hour).

238 Unbiased gene ontology (GO) analysis was used to identify biological processes associated
239 with the transcriptome of each immune cell cluster in the combined dataset. Top processes
240 associated with subsets were consistent with their phenotypic annotation, further validating
241 their identification as transcriptionally and functionally discrete immune cells (Figure S2A).
242 Monocytes were associated with 'wound healing' (Figure S2A(v)) macrophages with
243 phagocytosis (Figure S2A(vi)) and neutrophils with cell chemotaxis/migration (Figure
244 S2A(vii)).

245 To explore the functional role of monocytes, macrophages and neutrophils in endometrial
246 repair and remodelling, the expression of gene sets associated with essential tissue repair
247 processes, generated from literature searches and MsigDB [32], were interrogated in
248 scRNAseq data (Figure S2B). Neutrophils were found to have the highest expression of genes

249 associated with NETosis, chemoattraction and certain remodelling enzymes while
250 macrophages and monocytes expressed genes associated with phagocytosis. Notably, when
251 assessing the expression of genes associated with 'wound healing' each cell type showed
252 expression of a distinct subset of genes (monocytes: *Anxa5*, *Cav1*, *F10*, *Fn1*, *Pdpn*, *Sdc1*,
253 *Sdc4, Thbd*; macrophages: *Apoe*, *Axl*, *C3*, *Ccr2*, *Gnas*; neutrophils: *Slc11a1, Cd9, Lrg1, Plaur,*
254 *S100a9*) (Figure S3B). Taken together, GO analyses suggest that myeloid cells are
255 predominant during endometrial tissue repair and may have key role in wound healing
256 following menstruation.

257 *Flow cytometry analysis confirms dynamic changes in immune cell composition and the*
258 *predominance of myeloid cells during endometrial repair.*

259 To validate putative repair-associated changes in uterine immune cell composition identified
260 by *in silico* analyses, flow cytometry was performed on uterine tissues collected over a
261 comprehensive time course of endometrial repair using the mouse model of menstruation
262 (figure S1). A flow cytometry panel was designed to interrogate the immune cell populations
263 identified by scRNAseq using phenotypic markers as outlined in Supplementary Table 1.

264 Using the gating strategy outlined in figure 2A, flow cytometry analysis corroborated the
265 immune cell composition identified by scRNAseq analysis in cycling, repair (24 hr) and
266 remodelling (48 hr) tissues. This was complemented by analysis of additional time points
267 which provided resolution on immune cell dynamics prior to and during tissue breakdown
268 (Figure 2B & 2C). At 0 hr (prior to breakdown), there was an increase in the proportion of
269 monocytes within the uterus and a decrease in the proportion of NK cells and dendritic cells
270 (DCs) when compared to cycling control. At 12 hr during tissue breakdown there was a large
271 compositional shift characterised by a significant increase in the proportion of neutrophils in
272 the uterus, accounting for 87.82% ± 14.06 of all $CD45^+$ immune cells at this timepoint. The
273 proportion of neutrophils peaked at 24 hr (91.86% ± 2.60 of $CD45^+$ cells) during repair and
274 neutrophils were also the most abundant cell type at 48 hr (55.7% ± 12.72 of $CD45^+$ cells),

275 with the numbers of T cells, NK cells and macrophages also increasing at 48 hr (Figure 2B &
276 2C).

277 *Lymphocyte populations are infrequent during endometrial repair.*

278 T cells ($CD45^+$ $Ly6G^-$ $NK1.1^-$ $CD19^-$ $CD3^+$) were quantified in uterine tissue digests using flow
279 cytometry (Figure 3A). Both the relative abundance (percentage of $CD45^+$ cells) and absolute
280 numbers of T cells were significantly increased during tissue remodelling (48 hr; 8.52% ± 4.71
281 and 47.87 count/mg ± 27.80) when compared to earlier phases of breakdown (12 hr; 1.72% ±
282 3.84 and 8.06 count/mg ± 9.67) and repair (24 hr; 0.19% ± 0.13 and 11.77 count/mg ± 13.23)
283 (Figure 3B & 3C). IHC was performed on tissue samples from matching time points/conditions.
284 $CD3^+$ T cells were detected in the endometrium and myometrium of both 24- and 48-hour
285 tissues (Figure 3D; black arrows & Figure S4A). T cells were more readily detected in 48-hour
286 tissues but there was no spatially distinct distribution associated with different time-points
287 (Figure 3D; black arrows & Figure S4A).

288 NK cells ($CD45^+$ $Ly6G^-$ $CD3^-$ $CD19^-$ $NK1.1^+$) were more readily detected (Figure 3E) and
289 abundant in cycling mice (62.35 count/mg ± 120.30), numbers were lowest during breakdown
290 (12 hr; 9.069 count/mg ± 23.66) and repair (24 hr; 26.44 count/mg ± 30.64) but more abundant
291 in remodelling tissues (48 hr; 43.35 count/mg ± 32.52) (Figure 3G). Detection of NK cells using
292 DBA-lectin in uterine tissue sections located NK cells to the decidualised tissue prior to
293 breakdown (0-hour), in close proximity to the luminal epithelium and adjacent to the decidual-
294 endometrial boundary. In 24-hour tissues NK cells were infrequent, located predominantly in
295 the shed decidual tissue (Figure 3H) and in 48-hour tissues very few NK cells could be
296 detected (Figure S4B).

297 Quantitative analysis of B cells ($CD45^+$ $Ly6G^-$ $CD3^-$ $NK1.1^-$ $CD19^+$) demonstrated that B cells
298 are abundant in the uterus prior to breakdown (0 hr; 38.66 count/mg ± 24.97) but significantly
299 decreased thereafter (Figure 3J & 3K). Detection of $B220^+$ B cells in uterine tissue sections by
300 IHC showed B cells located in both the endometrium and myometrium prior to breakdown

301 (Figure 3L; 0 hr, black arrows) but they were infrequent during repair and remodelling (Figure
302 3L; black arrows & Figure S4C).

303 *Myeloid cell populations are dynamically regulated during endometrial breakdown, repair, and*
304 *remodelling.*

305 Flow cytometry and immunohistochemistry analyses demonstrated changes in the abundance
306 and location of key myeloid cell types in the uterus during endometrial repair. Monocytes
307 (Ly6C$^{+}$ MHCII$^{-}$; Figure 4A) were the most abundant immune cell present in the uterus prior to
308 breakdown (0-hour; 103.8 ± 50.46) (Figure 4B & 4C). The number of monocytes in the uterus
309 was then significantly decreased during breakdown when compared to prior to breakdown (0
310 hr; 103.80 count/mg ± 50.46 vs 12 hr; 25.40 count/mg ± 54.57, $p < 0.0001$). Monocytes were
311 significantly increased during repair (12 hr; 25.40 count/mg ± 54.57 vs 24 hr; 101.1 count/mg
312 ± 49.67, $p < 0.0001$) and significantly decreased during remodelling (24 hr; 101.1 count/mg ±
313 49.67 vs 48 hr; 10.44 count/mg ± 8.27, $p = 0.0018$) (Figure 4C). Immunofluorescent staining
314 was performed using an anti-CD14 antibody to investigate spatial distribution of monocytes in
315 uterine tissues. CD14$^{+}$ cells were predominantly localised to the boundary between the
316 underlying endometrium and the detached decidual tissue during breakdown (12 hr; Figure
317 S6A) and subsequent repair (24 hr; Figure 4J and Figure S6A).

318 Macrophages counts were significantly decreased during tissue breakdown when compared
319 to tissue repair (12 hr; 4.71 count/mg ± 8.17 vs 24 hr; 21.78 count/mg ± 26.47, $p = 0.0013$)
320 and remodelling time points (12 hr; 4.71 count/mg ± 8.17 vs 48 hr; 16.61 count/mg ± 10.69, p
321 < 0.0001) (Figure 4F). Macrophages (F4/80$^{+}$CD64$^{+}$; Figure 4D) were decreased during
322 endometrial repair but increased in the remodelling timepoint (24 hr; 0.36% ± 0.28 vs 48 hr;
323 2.80% ± 1.22, $p = 0.004$) (Figure 4E). CD64$^{+}$ macrophages were detected by
324 immunohistochemistry in all uterine tissue compartments throughout breakdown and repair
325 (0-24 hr; Figure S6B), in both the decidualised and non-decidualised endometrium, as well as
326 the myometrium. In 48-hour tissues, macrophages were most abundant in the stroma of the
327 remodelled endometrium (Figure 4K and Figure S6B).

328 Neutrophils (Ly6G$^+$SiglecF$^-$, Figure 4G) were the most abundant immune cell type present in
329 the uterus during breakdown (12 hr; 87.82% ± 14.06), repair (24 hr; 91.86% ± 2.60), and
330 remodelling (48 hr; 55.71% ± 12.72) (Figure 4H). Neutrophils counts in the uterus were
331 significantly increased during breakdown compared to cycling controls (12 hr; 1374 count/mg
332 ± 2398 vs cycling; 56.25 count/mg ± 175.80, $p < 0.0001$). Neutrophil abundance peaked during
333 endometrial repair (24 hr; 4946 count/mg ± 2344) and although neutrophil numbers were
334 relatively decreased during remodelling they were still significantly increased compared to
335 cycling controls (Figure 4I; cycling; 56.25 count/mg ± 175.80 vs 48 hr; 504.5 count/mg ± 570.6,
336 $p = 0.016$). Immunofluorescent staining identified abundant Ly6G$^+$ neutrophils in uterine
337 tissues during breakdown (12 hr) and repair (24 hr) specifically localised to the boundary
338 between the detached decidual tissue and the underlying endometrium (Figure S6C). In 48-
339 hour tissues, Ly6G$^+$ neutrophils were readily detected throughout the remodelled
340 endometrium (Figure S6C).

341 Dendritic cells (DCs; CD11c$^+$MHCII$^+$; Figure S5A) were infrequent during tissue breakdown
342 (12 hr; 5.63 count/mg ± 11.91) but were modestly increased during repair (24 hr; 15.80
343 count/mg ± 13.51) and remodelling (48 hr; 6.59 count/mg ± 6.019) (Figure S5B & S5C).
344 Eosinophils (Ly6G$^-$ SiglecF$^+$; Figure S5D) were infrequent in cycling tissues (3.26 count/mg ±
345 6.22) and during phases of tissue breakdown (12 hr; 2.14 count/mg ± 5.08) and repair (24 hr;
346 2.43 count/mg ± 4.20). Notably, eosinophils were significantly increased during remodelling
347 (48 hr; 17.60 count/mg ± 20.43) but were infrequent overall (Figure S5F). Due to their low
348 abundance, DCs and eosinophils were not analysed by IHC.

349 *Monocytes, neutrophils, and macrophages co-localise to areas of breakdown and tissue*
350 *repair.*

351 To understand the distribution of key myeloid cell types relative to each other in uterine tissue
352 sections, multiplex IHC for the detection of CD14 (monocytes), CD64 (macrophages) and
353 Ly6G (neutrophils) was performed using uterine tissues collected from across the time course
354 (Figure 4J-K, Figure S6D). Prior to tissue breakdown (0 hr), relatively few CD14$^+$ or Ly6G$^+$

355 cells could be detected but CD64$^+$ macrophages were abundant throughout the tissue (Figure
356 S6D). At 12 hr, during tissue breakdown, CD14$^+$ monocytes and Ly6G$^+$ neutrophils were
357 detected clustered within the same regions of the tissue and were localised to regions of
358 shedding, where decidualised tissue was detaching, as well as in the underlying residual
359 endometrium (Figure S5D). CD64$^+$ macrophages were located predominantly in the outer
360 myometrial layers at 12 hr and only diffusely detected within regions of tissue breakdown
361 (Figure S6D).

362 At 24 hr, CD14$^+$ monocytes and Ly6G$^+$ neutrophils were identified in the detaching decidual
363 tissue but were also detected in regions of underlying endometrium undergoing tissue repair
364 (Figure 4J & S6D). CD64$^+$ macrophages were also detected throughout the repairing
365 endometrium as well as in the decidual tissue, in association with regions where detachment
366 had not yet taken place (Figure 4J & S6D). At this time point, monocytes, neutrophils and
367 macrophages were detected within regions of active tissue repair but were less frequent in
368 areas of intact tissue. At 48 hr the decidual tissue is almost completely expelled, the luminal
369 epithelium is largely restored, and the underlying stroma is undergoing remodelling. CD14$^+$
370 monocytes were less frequent at 48 hr and localised only to regions of decidual detachment
371 on the endometrial surface, while Ly6G$^+$ neutrophils were abundant and dispersed throughout
372 the remodelling endometrium (Figure 4K & S6D). Notably, CD64$^+$ macrophages were more
373 abundant at 48 hr with an apparent expansion throughout the remodelling endometrium in
374 regions both proximal and distal to sites of recent tissue repair (Figure 4K & S6D).

375 *CellChat analysis of scRNAseq data identifies monocyte, macrophage and neutrophil*
376 *signalling pathways associated with endometrial repair.*

377 Given the association of monocytes, macrophages and neutrophils with tissue repair and
378 remodelling in the endometrium, further *in silico* analyses were performed to infer putative
379 signalling pathways and interactions associated with these cell types. CellChat analysis of
380 ligand-receptor expression was performed on scRNAseq data, and immune cell interactions
381 were assessed. Monocytes, macrophages and neutrophils were identified as both dominant

382 senders (high ligand expression) and dominant receivers (high receptor expression) in the
383 communication network, scoring highly in both outgoing and incoming interaction strength
384 (Figure 5A). The top signalling pathways found to contribute to outgoing/incoming signalling
385 across all immune cell types were CCL, CXCL, MIF, FN1, SPP1 and THBS (Figure 5B).
386 Analysis of communication patterns between cell types for these signalling pathways
387 highlighted the predominance of monocytes (CCL, CXCL, MIF, FN1, SPP1 and THBS),
388 macrophages (CCL, MIF and FN1) and neutrophils (CCL, CXCL, and THBS) as key
389 contributors to cell communication of repair-associated signalling pathways (Figure 5C).

390 The relationship between specific ligand-receptor pairs and immune cell subsets is
391 summarised in the chord diagrams for each signalling pathway, where the width of each chord
392 corresponds to the strength of the interaction (Figure 5D). The relationship between different
393 CCL chemokine ligands and corresponding receptors showed a predominance of ligand
394 expression associated with monocytes (*Ccl2*, *Ccl3*, *Ccl4*, *Ccl6* and *Ccl9*), macrophages (*Ccl2*,
395 *Ccl3*, *Ccl4*, *Ccl6 and Ccl9*) and neutrophils (*Ccl3*, *Ccl6* and *Ccl9*) (Figure 5Di). Crosstalk in
396 CXCL pathway was predominantly from monocytes and neutrophils signalling *Cxcl2* and *Cxcl3*
397 to *Cxcr2* on neutrophils and eosinophils (Figure 5Dii). *Mif* and *Fn1* signalled from monocytes
398 and macrophages to corresponding receptors on multiple cell types (Figure 5Diii and iv). *Spp1*
399 ligand was predominantly associated with monocytes signalling to distinct reciprocal receptors
400 including *Cd44* on neutrophils and integrins on monocytes and macrophages(Figure 5Dv).
401 Similarly, *Thbs1* signalling was predominantly from monocytes and neutrophils which
402 signalled via *Cd47* on all immune cell types in the dataset (Figure 5Dv and vi).

403 To examine the association of these signalling pathways more discretely, the top overall
404 signalling pathways were assessed for each experimental condition (Figure 5E). While similar
405 signalling pathways ranked highly, their association with specific immune cell subsets shifted
406 according to experimental conditions. The relative strength of THBS signalling was strongest
407 for neutrophils in cycling, but more strongly associated with monocytes in repair and
408 remodelling tissues. MIF signalling was strongly associated with DCs in cycling, but more

409 strongly associated with monocytes in repair, and with macrophages in remodelling tissues.
410 Notably, FN1 and SPP1 signalling was strongly associated with monocytes in all conditions.

411 Due to their strength of association with top signalling pathways, monocytes, macrophages
412 and neutrophils were extracted for further communication analyses (Figure 5F). Pairwise
413 comparisons between experimental conditions (cycling vs repair, cycling vs remodelling,
414 repair vs remodelling) revealed changes in THBS1, SPP1, MIF, CCL and CXCL signalling
415 pathways in monocytes, macrophages and neutrophils relative to phases of endometrial repair
416 and remodelling (Figure 5F). The greatest interaction strength for incoming and outgoing
417 signals in monocytes was associated with THBS1 in repair and SPP1 in remodelling.
418 Macrophage signalling also differed by condition with greatest signalling strength for THBS1
419 associated with repair while MIF and SPP1 were associated with remodelling. In each instance
420 these signalling pathways were associated with a large differential signal strength for both
421 incoming and outgoing interactions. Neutrophil signalling was also associated with THBS1
422 and SPP1 in repair and remodelling respectively. CCL signalling strength was reduced in
423 monocytes and macrophages but increased in neutrophils in remodelling. CXCL signalling
424 was strongly associated with neutrophils and both outgoing and incoming signalling strength
425 was upregulated during repair (24 hr) and remodelling (48 hr). Monocytes, macrophages and
426 neutrophils were strongly associated with THBS1 signalling during endometrial repair and
427 SPP1 and MIF signalling during remodelling. Chemokine signalling was distinctly associated
428 with neutrophils during remodelling consistent with roles in immune cell crosstalk and
429 recruitment at this time point.

430 Discussion

431 In this study, we combined a mouse model of menstruation with comprehensive immune cell
432 profiling to characterise the contribution of distinct immune subsets to endometrial repair. We
433 found that uterine immune cell composition was dynamic, with pronounced temporal and
434 spatial changes in monocytes, macrophages and neutrophils which were associated with
435 regions of tissue repair and remodelling. These data suggest that monocyte and neutrophil
436 infiltration is a key feature of endometrial repair, typical of early inflammation responses
437 observed in other tissue contexts[33, 34]. Neutrophils, typically associated with acute
438 inflammatory responses, were abundant during tissue repair as well as remodelling, while
439 macrophages, which regulate tissue repair processes, were relatively decreased during active
440 repair. Myeloid cells were enriched for both pro- and anti-inflammatory signalling pathways,
441 highlighting the discrete balance of immune cell functions that support this unique repair
442 process. Utilising scRNAseq data we were able to identify key signalling pathways associated
443 with myeloid cells during menstruation which included THBS1 and SPP1 as important
444 mediators of endometrial repair. Collectively, these data provide new insights into the
445 immunology of menstruation and highlight specific spatiotemporal roles for myeloid cells
446 during endometrial repair.

447 We found that monocytes and macrophages were transcriptionally similar with overlapping
448 expression of markers such as *Csf1r*, *Cd68*, *Msr1* and *Fn1*. However, *Inha* and *Cxl3*
449 expression was distinct to monocytes consistent with potential roles in regulating migration
450 and adhesion of inflammatory cells to sites of tissue repair [35]. GOBP analysis highlighted
451 enrichment for genes associated with wound healing and endoplasmic reticulum stress.
452 Monocytes expressed apoptosis- and phagocytosis-associated genes as well as a subset of
453 wound healing genes, such as *Pdpn* and *Cav1*, that were distinct from those expressed by
454 macrophages and neutrophils. Specifically, *Cav1* expression has been shown to increase
455 during monocyte adhesion and drives monocyte-to-macrophage differentiation [36].

456 CD14+ monocytes were located in both the decidualised tissue and underlying endometrium
457 and were detected in close association with macrophages and neutrophils. Cell chat analysis
458 identified monocytes as major drivers of intercellular communication in the uterus with the
459 highest incoming and outgoing signalling strength amongst immune cells, followed by
460 macrophages and neutrophils. Monocytes were associated with signalling via CCL, MIF,
461 SPP1 and THBS and were the predominant outgoing signal source for these signalling
462 pathways. Signalling via THBS and SPP1 was strongly associated with monocytes from repair
463 and remodelling tissues, respectively.

464 SPP1 (Secreted Phosphoprotein 1, also known as Osteopontin) plays multiple roles in tissue
465 repair and is reported to modulate inflammation and tissue remodelling. SPP1 mediates cell-
466 to-cell and cell-to-matrix interactions, via integrins and CD44, which can promote macrophage
467 migration and effector functions[37]. SPP1 also increases expression of S100A9, IL-1β, and
468 chemokines like CCL2, CCL3 and CCL4 which skews monocytes toward a pro-inflammatory
469 phenotype[38]. Notably, these genes were enriched in the transcriptome of uterine monocytes
470 during menstruation in the current study. Thrombospondin 1 (TSP-1) promotes cell migration
471 and tissue remodelling via TGF-β and integrin signalling which may support tissue repair in
472 the endometrium [39] [40]. However, it can also inhibit repair by suppressing angiogenesis, a
473 crucial component of endometrial repair [41]. TSP-1 signalling was enriched in monocytes
474 from repair tissues, but the signal strength was relatively decreased in remodelling tissues,
475 when vascular remodelling is more prominent, highlighting the discrete and dynamic
476 contributions of different inflammatory cells and mediators to endometrial repair during
477 menstruation.

478 We have previously shown that distinct subsets of macrophages associate with regions
479 endometrial repair during menstruation [16] but the function/phenotype of uterine
480 macrophages has not been elucidated. In the current study, we found that macrophages were
481 enriched for signalling pathways important for tissue repair and remodelling. This included
482 complement pathway which has roles in clearing cellular debris, recruiting immune cells to

483 sites of injury, releasing growth factors and regulating blood clotting in tissue repair processes.
484 Differential gene expression analysis highlighted that uterine macrophages distinctly
485 expressed key components of the complement pathway, including *C1qa*, which is a marker of
486 tissue resident macrophages in other contexts [42]. Macrophages were also enriched for
487 genes involved in galectin signalling indicative of a pro-resolving phenotype [43]. Similar to
488 monocytes, macrophages were also associated with MIF and FN1 signalling networks which
489 were key pathways of cell-cell communication. The transcriptomic similarities between
490 macrophages and monocytes are likely representative of linked differentiation trajectories
491 within uterine tissues. Although the ontogeny and kinetics of monocytes and macrophages in
492 the uterus are yet to be fully defined, studies using tissue explants, or organ transplants,
493 suggest the uterine macrophage niche is maintained via monocyte-driven replenishment [44,
494 45]. This is consistent with the compositional changes in macrophages and monocytes
495 described in the current study, where monocytes are predominant during repair, but
496 macrophages, likely monocyte-derived, are more abundant than monocytes during
497 remodelling.

498 ScRNAseq data analysis confirmed that neutrophils were a major source of chemokines as
499 they were enriched for both CCL and CXCL-mediated signalling pathways, indicating
500 regulation of immune cell recruitment within the repairing endometrium. Neutrophils were
501 associated with pro-inflammatory signalling via TNF pathways, which, interestingly, was
502 prominent during remodelling rather than repair. While TNF is a classic pro-inflammatory
503 mediator, Annexin1 signalling was also enriched in neutrophils at this timepoint. Annexin1 has
504 anti-inflammatory functions by downregulating neutrophil activation [46, 47]. The neutrophil
505 transcriptome profile was consistently associated with both pro- and anti-inflammatory
506 pathways which may suggest neutrophil phenotype is temporally altered in the uterine tissue
507 environment across repair and remodelling, with a switch to anti-inflammatory functions during
508 the latter phase. Assessing differentially expressed genes in neutrophils highlighted that in
509 addition to classic neutrophils markers such as *S100a8*, *S100a9* and *Cxcl2*, uterine

510 neutrophils also expressed *Dusp1* and *Acod1* indicating an anti-inflammatory phenotype.
511 Notably, Dusp1 (Dual Specificity Phosphatase 1) has key roles in resolution of inflammation
512 by deactivating pro-inflammatory mitogen-activated protein kinase (MAPK)-dependent
513 pathways and influencing production of neutrophil chemoattractants like Cxcl1[48]. This may
514 reflect a functional requirement for restraining classic effector functions of neutrophils within
515 the uterus in the context of endometrial repair. Expression of Acod1 (Aconitate Decarboxylase
516 1) in neutrophils regulates inflammation via production of itaconate. This shift in
517 immunometabolism is associated with anti-inflammatory protein production, protecting cells
518 from oxidative stress as well as regulation of NET formation and neutrophil migration [49, 50].
519 Thus, although neutrophils are abundant during menstruation, their transcriptomic phenotype
520 supports roles in coordinating immune responses via chemokine secretion and promoting
521 resolution of inflammation through suppression of pro-inflammatory signalling pathways.
522 Transcriptome profiling in the current study supports reparative functions for neutrophils during
523 menstruation consistent with emerging roles for neutrophils in contributing to tissue repair in
524 other contexts [51-53]. Indeed, Kaitu'u-Lino et al. previously demonstrated the importance of
525 monocytes and macrophages to endometrial breakdown and repair using antibody-based
526 depletion (RB6-8C5) of Gr-1 positive cells in a mouse model of menstruation [54].

527 Our findings using a mouse model of simulated menstruation extend and complement those
528 from analysis of human endometrial tissues. Armstrong et al., investigated mRNA expression
529 levels of inflammatory cytokines and chemokines during menstruation in the human
530 endometrium and found increased expression of CCL2, CXCL8, IL6 and TNF during the
531 menstrual phase of the cycle[8]. Importantly, the current study provides much needed
532 resolution to the specific cellular sources of these mediators which may be beneficial to
533 translational studies aiming to understand the pathophysiology of menstrual dysfunction in
534 reproductive health disorders. Dysregulated inflammatory responses are a common feature of
535 reproductive health disorders such as heavy menstrual bleeding (HMB) and endometriosis,
536 with changes to macrophage and neutrophil function reported[55]. While studies

537 characterising specific phenotypes of immune cell subsets during menstruation are lacking,
538 changes in expression to key mediators described in the current study have been reported.
539 For example, TSP-1 expression is reported to be decreased in endometrial tissues from
540 women with HMB [41] while overexpression of SPP1 has been reported in macrophages from
541 women with endometriosis[56]. Further research will be needed to better characterise immune
542 dysfunction in human reproductive disorders, but the comprehensive phenotyping performed
543 in the current study provides tractable targets for further translational investigation.

544 Conclusion

545 Here, we have comprehensively profiled immune cells using a combination of scRNAseq, flow
546 cytometry and multiplex immunohistochemistry and identified that monocytes, macrophage
547 and neutrophils are spatially and temporally regulated to support endometrial repair. These
548 data provide a more complete understanding of how different immune cell populations
549 contribute to endometrial tissue repair and identify key cell-specific mediators and pathways.
550 Future studies should assess the importance of myeloid cells to endometrial repair through
551 lineage tracing, cell ablation and comparison to human datasets. Improved understanding of
552 endometrial repair will, in turn, support identification of potential pathways that are
553 dysregulated in reproductive health disorders in women.

554 References


555 1. Critchley, H.O., et al., *The endocrinology of menstruation--a role for the immune*
556 *system.* Clin Endocrinol (Oxf), 2001. **55**(6): p. 701-10.
557 2. Critchley, H.O.D., et al., *Physiology of the Endometrium and Regulation of*
558 *Menstruation.* Physiol Rev, 2020. **100**(3): p. 1149-1179.
559 3. Kirkwood, P.M., I.W. Shaw, and P.T.K. Saunders, *Mechanisms of Scarless Repair at*
560 *Time of Menstruation: Insights From Mouse Models.* Front Reprod Health, 2021. **3**: p.
561 801843.
562 4. Maybin, J.A. and H.O. Critchley, *Steroid regulation of menstrual bleeding and*
563 *endometrial repair.* Rev Endocr Metab Disord, 2012. **13**(4): p. 253-63.
564 5. Hu, X., et al., *Cyclical endometrial repair and regeneration: Molecular mechanisms,*
565 *diseases, and therapeutic interventions.* MedComm (2020), 2023. **4**(6): p. e425.
566 6. Lee, S.K., et al., *Immune cells in the female reproductive tract.* Immune Netw, 2015.
567 **15**(1): p. 16-26.
568 7. Lathbury, L.J. and L.A. Salamonsen, *In-vitro studies of the potential role of neutrophils*
569 *in the process of menstruation.* Mol Hum Reprod, 2000. **6**(10): p. 899-906.
570 8. Armstrong, G.M., et al., *Endometrial apoptosis and neutrophil infiltration during*
571 *menstruation exhibits spatial and temporal dynamics that are recapitulated in a mouse*
572 *model.* Sci Rep, 2017. **7**(1): p. 17416.
573 9. White, H.D., et al., *CD3+ CD8+ CTL activity within the human female reproductive*
574 *tract: influence of stage of the menstrual cycle and menopause.* J Immunol, 1997.
575 **158**(6): p. 3017-27.
576 10. Chen, C.K., et al., *Increased expressions of CD69 and HLA-DR but not of CD25 or*
577 *CD71 on endometrial T lymphocytes of nonpregnant women.* Hum Immunol, 1995.
578 **42**(3): p. 227-32.
579 11. Flynn, L., et al., *Menstrual cycle dependent fluctuations in NK and T-lymphocyte*
580 *subsets from non-pregnant human endometrium.* Am J Reprod Immunol, 2000. **43**(4):
581 p. 209-17.
582 12. Starkey, P.M., L.M. Clover, and M.C. Rees, *Variation during the menstrual cycle of*
583 *immune cell populations in human endometrium.* Eur J Obstet Gynecol Reprod Biol,
584 1991. **39**(3): p. 203-7.
585 13. Chen, K., et al., *Single-cell transcriptomic analysis of immune cell dynamics in the*
586 *healthy human endometrium.* Biochem Biophys Rep, 2024. **39**: p. 101802.
587 14. Wang, W., et al., *Single-cell transcriptomic atlas of the human endometrium during the*
588 *menstrual cycle.* Nat Med, 2020. **26**(10): p. 1644-1653.
589 15. Cousins, F.L., et al., *Evidence from a mouse model that epithelial cell migration and*
590 *mesenchymal-epithelial transition contribute to rapid restoration of uterine tissue*
591 *integrity during menstruation.* PLoS One, 2014. **9**(1): p. e86378.
592 16. Cousins, F.L., et al., *Evidence for a dynamic role for mononuclear phagocytes during*
593 *endometrial repair and remodelling.* Sci Rep, 2016. **6**(1): p. 36748.
594 17. Salamonsen, L.A., et al., *Regulation of matrix metalloproteinases in human*
595 *endometrium.* Hum Reprod, 2000. **15 Suppl 3**: p. 112-9.
596 18. Thiruchelvam, U., et al., *The importance of the macrophage within the human*
597 *endometrium.* J Leukoc Biol, 2013. **93**(2): p. 217-25.
598 19. Tabibzadeh, S. and X.Z. Sun, *Cytokine expression in human endometrium throughout*
599 *the menstrual cycle.* Hum Reprod, 1992. **7**(9): p. 1214-21.
600 20. Jones, R.L., et al., *Identification of chemokines important for leukocyte recruitment to*
601 *the human endometrium at the times of embryo implantation and menstruation.* J Clin
602 Endocrinol Metab, 2004. **89**(12): p. 6155-67.

603 21. Crona Guterstam, Y., et al., *The cytokine profile of menstrual blood.* Acta Obstet
604 Gynecol Scand, 2021. **100**(2): p. 339-346.
605 22. Hampton, A.L. and L.A. Salamonsen, *Expression of messenger ribonucleic acid*
606 *encoding matrix metalloproteinases and their tissue inhibitors is related to*
607 *menstruation.* J Endocrinol, 1994. **141**(1): p. R1-3.
608 23. Sharkey, A.M., et al., *Vascular endothelial growth factor expression in human*
609 *endometrium is regulated by hypoxia.* J Clin Endocrinol Metab, 2000. **85**(1): p. 402-9.
610 24. Kirkwood, P.M., et al., *Single-cell RNA sequencing redefines the mesenchymal cell*
611 *landscape of mouse endometrium.* FASEB J, 2021. **35**(4): p. e21285.
612 25. Kirkwood, P.M., et al., *Single-cell RNA sequencing and lineage tracing confirm*
613 *mesenchyme to epithelial transformation (MET) contributes to repair of the*
614 *endometrium at menstruation.* Elife, 2022. **11**.
615 26. Stuart, T. and R. Satija, *Integrative single-cell analysis.* Nat Rev Genet, 2019. **20**(5): p.
616 257-272.
617 27. Wolock, S.L., R. Lopez, and A.M. Klein, *Scrublet: Computational Identification of Cell*
618 *Doublets in Single-Cell Transcriptomic Data.* Cell Syst, 2019. **8**(4): p. 281-291 e9.
619 28. Core, H.C.B. *Elbow plot: Quantitative approach*. Introduction to Single-cell RNA-seq
620 - ARCHIVED. ; Available from: https://hbctraining.github.io/scRNA-
621 seq/lessons/elbow_plot_metric.html.
622 29. Yu, G., et al., *clusterProfiler: an R package for comparing biological themes among*
623 *gene clusters.* OMICS, 2012. **16**(5): p. 284-7.
624 30. Jin, S., et al., *Inference and analysis of cell-cell communication using CellChat.* Nat
625 Commun, 2021. **12**(1): p. 1088.
626 31. Edgar, R., M. Domrachev, and A.E. Lash, *Gene Expression Omnibus: NCBI gene*
627 *expression and hybridization array data repository.* Nucleic Acids Res, 2002. **30**(1): p.
628 207-10.
629 32. Liberzon, A., et al., *The Molecular Signatures Database (MSigDB) hallmark gene set*
630 *collection.* Cell Syst, 2015. **1**(6): p. 417-425.
631 33. Kolaczkowska, E. and P. Kubes, *Neutrophil recruitment and function in health and*
632 *inflammation.* Nat Rev Immunol, 2013. **13**(3): p. 159-75.
633 34. Serbina, N.V., et al., *Monocyte-mediated defense against microbial pathogens.* Annu
634 Rev Immunol, 2008. **26**(Volume 26, 2008): p. 421-52.
635 35. Petraglia, F., et al., *Inhibin and activin modulate human monocyte chemotaxis and*
636 *human lymphocyte interferon-gamma production.* J Clin Endocrinol Metab, 1991.
637 **72**(2): p. 496-502.
638 36. Fu, Y., et al., *Caveolin-1 plays a critical role in the differentiation of monocytes into*
639 *macrophages.* Arterioscler Thromb Vasc Biol, 2012. **32**(9): p. e117-25.
640 37. Kitano, T., et al., *Transcriptome Analysis Identified SPP1-Positive Monocytes as a Key*
641 *in Extracellular Matrix Formation in Thrombi.* J Am Heart Assoc, 2025. **14**(19): p.
642 e044299.
643 38. MacDonald, L., et al., *COVID-19 and RA share an SPP1 myeloid pathway that drives*
644 *PD-L1+ neutrophils and CD14+ monocytes.* JCI Insight, 2021. **6**(13).
645 39. Wilson, Z.S., et al., *Critical role of thrombospondin-1 in promoting intestinal mucosal*
646 *wound repair.* JCI Insight, 2024. **9**(17).
647 40. Streit, M., et al., *Thrombospondin-1 suppresses wound healing and granulation tissue*
648 *formation in the skin of transgenic mice.* EMBO J, 2000. **19**(13): p. 3272-82.
649 41. Rae, M., et al., *Cortisol inactivation by 11beta-hydroxysteroid dehydrogenase-2 may*
650 *enhance endometrial angiogenesis via reduced thrombospondin-1 in heavy*
651 *menstruation.* J Clin Endocrinol Metab, 2009. **94**(4): p. 1443-50.

42. Horowitz, A., et al., *C1QA is an invariant biomarker for tissue macrophages.* bioRxiv, 2024.
43. Yaseen, H., et al., *Galectin-1 Facilitates Macrophage Reprogramming and Resolution of Inflammation Through IFN-beta.* Front Pharmacol, 2020. **11**: p. 901.
44. Bister, J., et al., *Tissue-specific nonheritable influences drive endometrial immune system variation.* Sci Immunol, 2024. **9**(94): p. eadj7168.
45. Guo, Y., et al., *Comprehensive analysis of leukocytes, vascularization and matrix metalloproteinases in human menstrual xenograft model.* PLoS One, 2011. **6**(2): p. e16840.
46. Sugimoto, M.A., et al., *Annexin A1 and the Resolution of Inflammation: Modulation of Neutrophil Recruitment, Apoptosis, and Clearance.* J Immunol Res, 2016. **2016**(1): p. 8239258.
47. Guido, B.C., et al., *Annexin-A1 peptide down-regulates the leukocyte recruitment and up-regulates interleukin-10 release into lung after intestinal ischemia-reperfusion in mice.* J Inflamm (Lond), 2013. **10**(1): p. 10.
48. Hoppstadter, J. and A.J. Ammit, *Role of Dual-Specificity Phosphatase 1 in Glucocorticoid-Driven Anti-inflammatory Responses.* Front Immunol, 2019. **10**: p. 1446.
49. Ji, J., et al., *IRG1/ACOD1 promotes neutrophil reverse migration and alleviates local inflammation.* J Leukoc Biol, 2024. **116**(4): p. 854-863.
50. Zhao, N., et al., *Neutrophil Irg1/itaconate axis protects against experimental colitis by suppressing local inflammation and maintaining hematopoietic homeostasis.* Mol Biomed, 2025. **6**(1): p. 143.
51. Rizo-Tellez, S.A. and J.G. Filep, *Beyond host defense and tissue injury: the emerging role of neutrophils in tissue repair.* Am J Physiol Cell Physiol, 2024. **326**(3): p. C661-C683.
52. Peiseler, M. and P. Kubes, *More friend than foe: the emerging role of neutrophils in tissue repair.* J Clin Invest, 2019. **129**(7): p. 2629-2639.
53. Loh, W. and S. Vermeren, *Anti-Inflammatory Neutrophil Functions in the Resolution of Inflammation and Tissue Repair.* Cells, 2022. **11**(24).
54. Kaitu'u-Lino, T.J., N.B. Morison, and L.A. Salamonsen, *Neutrophil depletion retards endometrial repair in a mouse model.* Cell Tissue Res, 2007. **328**(1): p. 197-206.
55. Wilson, T.R., S. Kasper, and K.A. Burns, *An emerging role for neutrophils in the pathogenesis of endometriosis.* 2025. **3**(1): p. 9.
56. Zhang, S., et al., *SPP1 as a key modulator of M2 macrophage polarization promotes endometriosis progression via activation of the FAK/PI3K/AKT pathway: A bioinformatics and experimental study.* Int Immunopharmacol, 2025. **166**: p. 115563.

691 Acknowledgments

692 *General*

693 We are sincerely grateful to the members of the SURF imaging suite at the University of
694 Edinburgh and the Veterinary and other staff in Biological Services for their assistance. Flow
695 cytometry data were generated with support from the IRR Flow Cytometry and cell sorting
696 facility, University of Edinburgh.

697 For the purpose of open access, the author has applied a Creative Commons Attribution (CC
698 BY) licence to any Author Accepted Manuscript version arising from this submission.

699 *Funding*

700 This work was supported by the Wellcome Trust (Fellowship 220656/Z/20/Z to DAG), and the
701 Medical Research Council studentship (MR/W006804/1; RJA/DAG).

702 *Author contributions*

703 Conceptualization: DAG

704 Methodology: RJA, PMK, HL, SG, IS, DAG

705 Analysis: RJA, PMK, HL, SG, IS, DAG

706 Funding acquisition: DAG

707 Writing – original draft: RJA, PMK, IS, DAG

708 Writing – review & editing: RJA, PMK, PTKS, IS, DAG

709 *Data and materials*

710 All data are available in the main text or the supplementary materials

711

712 Figures

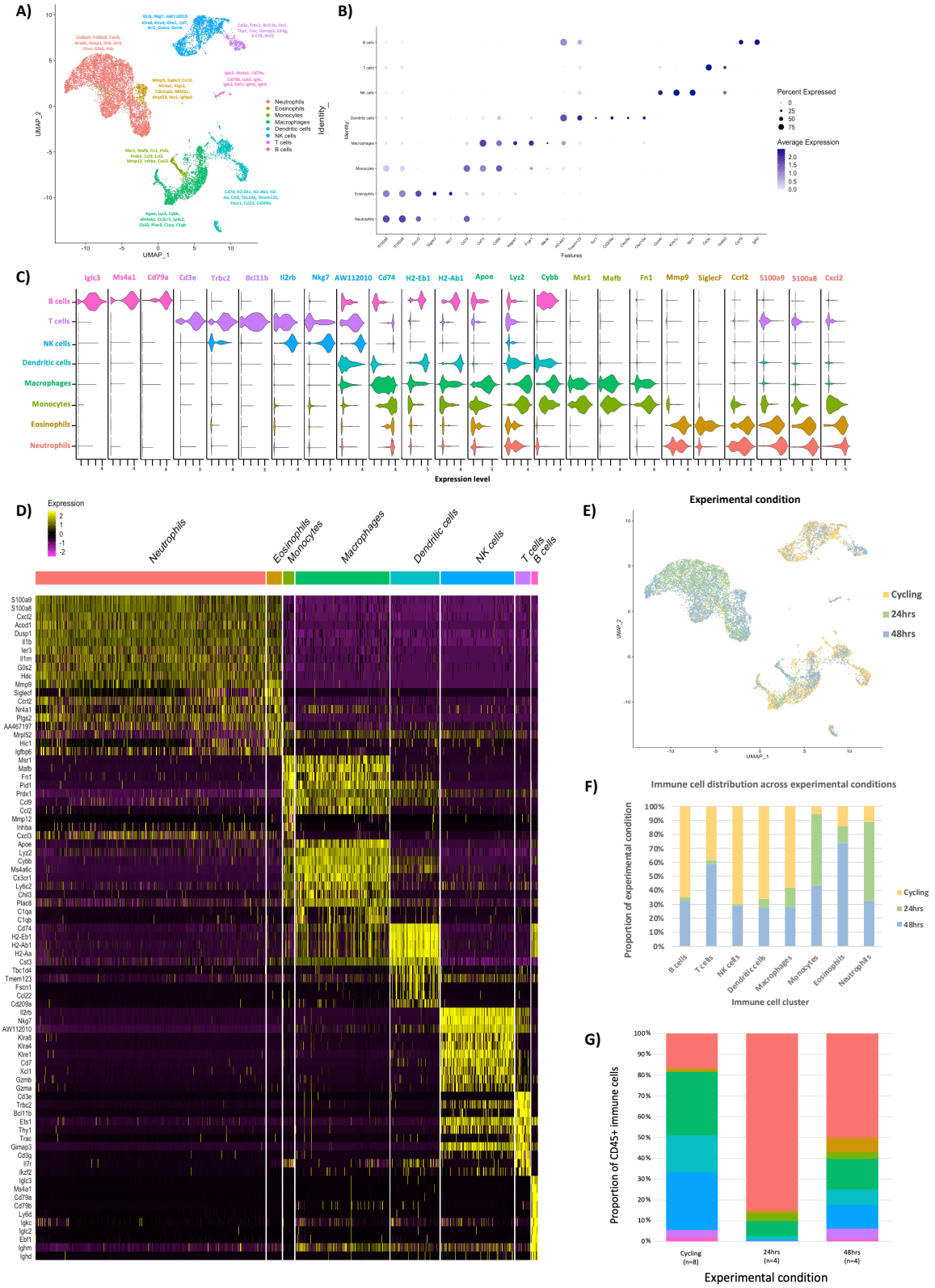


713

714 **Figure 1: Single cell RNA sequencing analysis identifies 8 uterine immune cell**
715 **populations in a mouse model of endometrial repair.**

716 **(A)** Uniform manifold approximation and projection (UMAP) visualisation: population restricted
717 $CD45^+$ immune cells isolated from mouse uterine tissue samples taken from steady state
718 control mice (cycling, n=8) and menstruating mice 24- (endometrial repair, n=4) and 48 hr
719 (endometrial remodelling, n=4) after progesterone withdrawal. **(B)** Dot plot: Expression of
720 canonical immune cell markers: neutrophils (*S100a8*, *S100a9*, *Cxcr2*), eosinophils (*SiglecF*,
721 *Hic1*), monocytes (*Cd14*), macrophages (*Csfr1, Cd68, Adgre1*, *Fcgr1, Mertk*), dendritic cells
722 (*H2-Ab1, Tmem123, Xcr1, Cd209a, Clec9a, Clec10a*), natural killer cells (*Gzmb, Klrb1c,*
723 *Ncr1*), T cells (*Cd3e, Gata3*), and B cells (*Cd19, Ighd*). Dot size: percentage of cells in each
724 cluster expressing the gene; Dot colour: average expression per cluster from low (lavender)
725 to high (dark blue). **(C)** Violin plot: Expression of the top 3 differentially expressed genes in
726 each cell cluster displayed as log ($TPM^+1$). TPM= transcript count per million. **(D)** Heatmap
727 (yellow, high; purple, low): Top 10 differentially expressed genes in each cell cluster (logFC >
728 0.5, p-value <0.05, Wilcoxon rank-sum test). Top axis is colour coded and named by immune
729 cell type. **(E)** Feature plot: Distribution of cells from each experimental condition. **(F)** Bar plot:
730 Summary of immune cell origin across experimental conditions. Each colour represents each
731 experimental condition, and the y-axis denotes the contribution of each experimental condition
732 to each immune cell cluster. **(G)** Stacked bar plot: Single cell RNA sequencing analysis of the
733 relative abundance of uterine immune cell populations during endometrial repair. Each colour
734 represents a distinct immune cell type, and the y-axis denotes the percentage of total $CD45^+$
735 immune cells.

736

A)

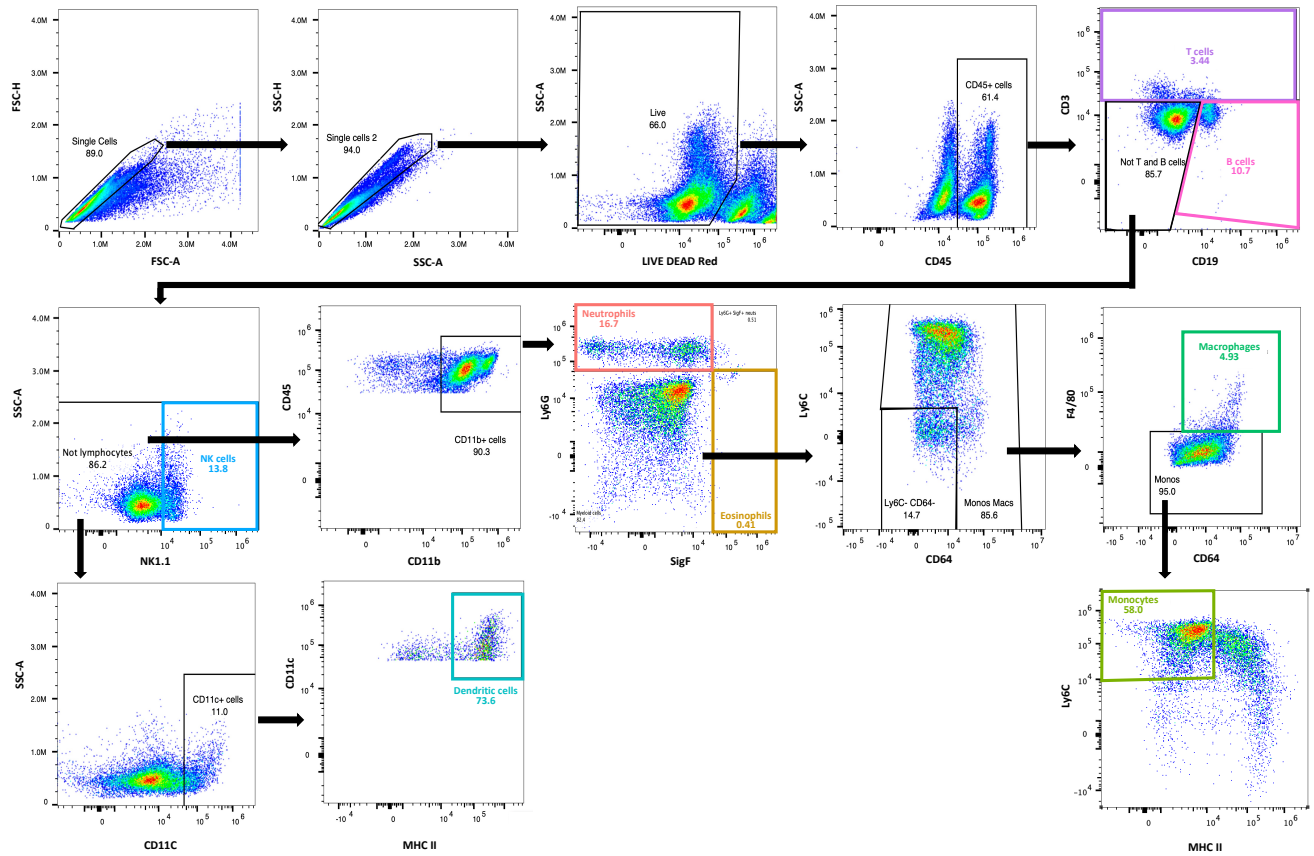


B) Flow cytometry – Relative abundance of CD45⁺ cells

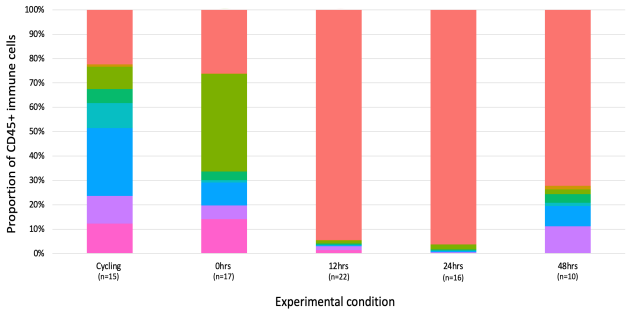


C) Flow cytometry – Relative abundance of CD45⁺ cells

| Cycling (Steady state) | 0hrs (Prior to breakdown) | 12hrs (Breakdown) | 24hrs (Repair) | 48hrs (Remodel) | Cluster |
|---|---|---|---|---|---|
| 8.627 | 8.458 | 1.310 | 0.107 | 0.161 | B cells |
| 5.477 | 3.266 | 1.410 | 0.189 | 8.519 | T cells |
| 16.326 | 5.626 | 0.316 | 0.415 | 6.468 | NK cells |
| 7.235 | 0.648 | 0.277 | 0.269 | 0.996 | Dendritic cells |
| 4.114 | 2.074 | 0.351 | 0.361 | 2.801 | Macrophages |
| 6.477 | 24.100 | 1.248 | 1.976 | 1.477 | Monocytes |
| 0.680 | 0.075 | 0.198 | 0.034 | 1.151 | Eosinophils |
| 15.788 | 15.776 | 87.818 | 91.856 | 55.710 | Neutrophils |

**Figure 2: Flow cytometry analysis reveals dynamics changes in uterine immune cell composition during a mouse model of endometrial repair and remodelling. (A)** Flow cytometry gating strategy employed to identify and quantify distinct immune cell populations in uterine tissue digests. **(B)** Stacked bar plot: relative abundance of uterine immune cell populations across phases of endometrial repair and remodelling (0-,12-, 24-, 48 hr following progesterone withdrawal) compared to cycling/steady state control tissue: colours represent distinct immune cell types, and the y-axis denotes the percentage of total CD45⁺ immune cells

745 in each dataset. **(C)** Table: Quantification of flow cytometry analysis of the relative abundance
746 of uterine immune cell populations across phases of endometrial repair and remodelling: 0 hr
747 (n=17), 12 hr (n=22), 24 hr (n=16) and 48 hr (n=10) following progesterone withdrawal
748 compared to cycling/steady state control tissue (n=15).

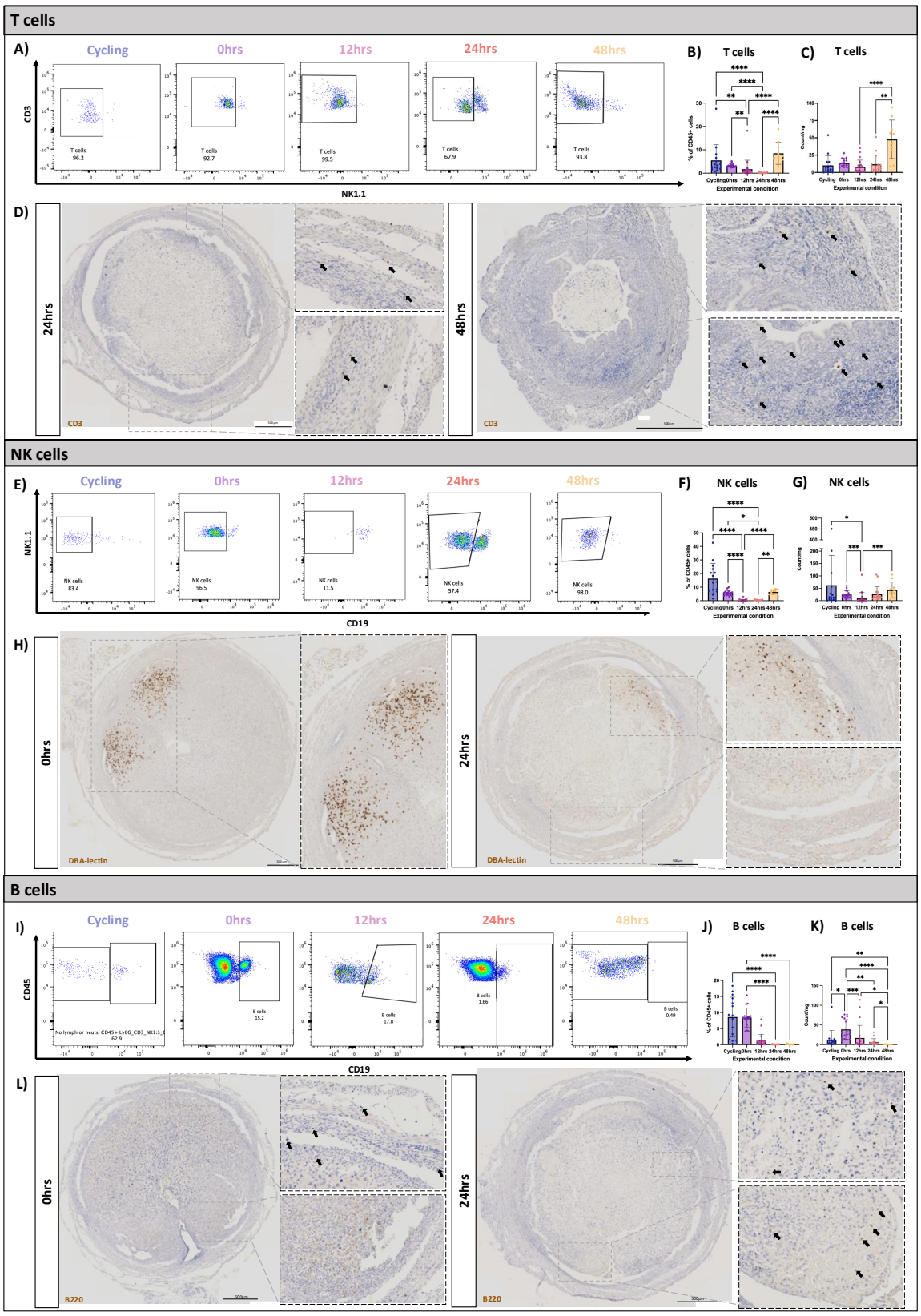


**Figure 3: Flow cytometry and immunohistochemistry reveal dynamic changes in uterine lymphocyte populations during endometrial repair using a mouse model of**

752 **simulated menstruation. (A)** Population restricted FC analysis to identify $CD45^+$ $Ly6G^-$
753 $NK1.1^-$ $CD19^-$ $CD3^+$ T cells in uterine tissue digests. **(B)** Bar plot, FC quantification: Relative
754 abundance of T cells calculated as a percentage of total $CD45^+$ cells per uterine horn. **(C)** Bar
755 plot, FC quantification: Absolute counts of T cells per uterine horn. **(D)** Immunohistochemistry:
756 detection of $CD3^+$ T cells (black arrows) in uterine tissues 24- and 48 hr after progesterone
757 withdrawal (representative images: 24 hr n=5, 48 hr n=6, scale bar= 50μm). **(E)** Population
758 restricted FC analysis to identify $CD45^+$ $Ly6G^-$ $CD3^-$ $CD19^-$ $NK1.1^+$ NK cells in uterine tissue
759 digests. **(F)** Bar plot, FC quantification: Relative abundance of NK cells calculated as a
760 percentage of total $CD45^+$ cells per uterine horn. **(G)** Bar plot, FC quantification: Absolute
761 counts of NK cells per uterine horn. **(H)** Immunohistochemistry: detection of DBA-bound NK
762 cells in uterine tissues 24- and 48 hr after progesterone withdrawal (representative images:
763 24 hr n=4, 48 hr n=4, scale bar= 50μm). **(I)** Population restricted FC analysis to identify $CD45^+$
764 $Ly6G^-$ $CD3^-$ $NK1.1^-$ $CD19^+$ B cells in uterine tissue digests **(J)** Bar plot, FC quantification:
765 Relative abundance of B cells calculated as a percentage of total $CD45^+$ cells per uterine horn.
766 **(K)** Bar plot, FC quantification: Absolute counts of B cells per uterine horn. **(L)**
767 Immunohistochemistry: detection of $B220^+$ B cells (black arrows) in uterine tissues 24- and 48
768 hr after progesterone withdrawal (representative images: 24 hr n=4, 48 hr n=4, scale bar=
769 50μm). (FC analysis groups: control (n=15), 0 hr (prior to breakdown, n=17), 12 hr (tissue
770 breakdown, n=22), 24 hr (tissue repair, n=16) and 48 hr (tissue remodelling, n=10) after
771 progesterone withdrawal; statistical comparisons were made using Kruskal-Wallis tests with
772 multiple comparisons. * $p< 0.05$, ** $p < 0.01$, *** $p < 0.001$, **** $p < 0.0001$).

773

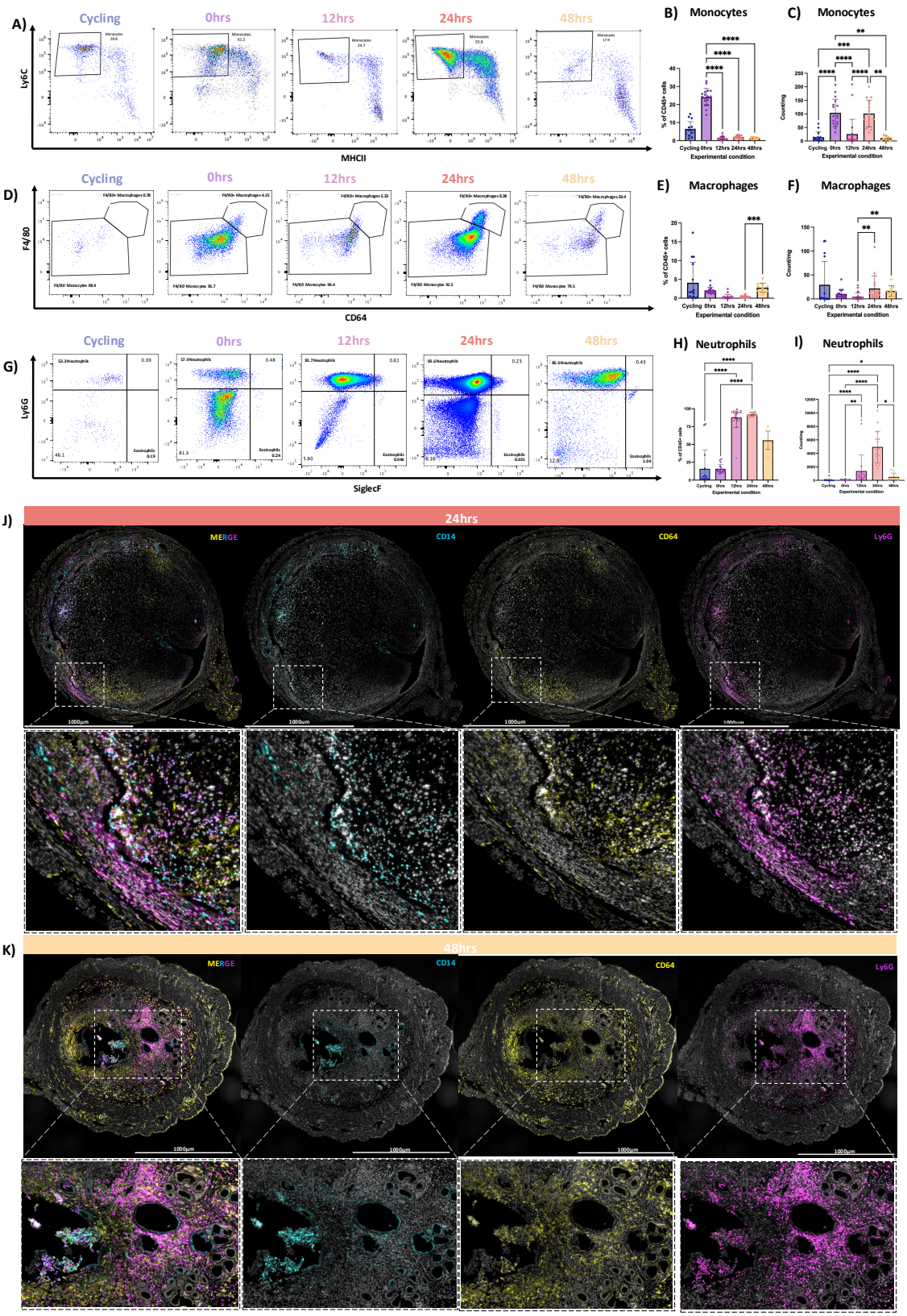


774

775 **Figure 4: Flow cytometry and immunohistochemistry reveal dynamic changes in**

776 **uterine myeloid cell populations during endometrial repair using a mouse model of**

**simulated menstruation. (A)** Population restricted FC analysis to identify $CD45^+$ $CD3^-$ $CD19^-$ $NK1.1^-$ $CD11b^+$ $Ly6G^-$ $SiglecF^-$ $CD64^-$ $Ly6C^+$ $MHCII^-$ monocytes in uterine tissue digests. **(B)** Bar plot, FC quantification: Relative abundance of monocytes calculated as a percentage of total $CD45^+$ cells per uterine horn. **(C)** Bar plot, FC quantification: Absolute counts of monocytes per uterine horn. **(D)** Population restricted FC analysis of $CD45^+$ $CD3^-$ $CD19^-$ $NK1.1^-$ $CD11b^+$ $Ly6G^-$ $SiglecF^-$ $CD64^+$ $Ly6C^-$ $F4/80^+$ $MHCII^+$ macrophages in uterine tissue digests. **(E)** Bar plot, FC quantification: Relative abundance of macrophages calculated as a percentage of total $CD45^+$ cells per uterine horn. **(F)** Bar plot, FC quantification: Absolute counts of macrophages per uterine horn . **(G)** Population restricted FC analysis of $CD45^+$ $CD3^-$ $CD19^-$ $NK1.1^-$ $CD11b^+$ $Ly6G^+$ $SiglecF^-$ neutrophils in uterine tissue digests. **(H)** Bar plot, FC quantification: Relative abundance of neutrophils calculated as a percentage of total $CD45^+$ cells per uterine horn. **(I)** Bar plot, FC quantification: Absolute counts of neutrophils per uterine horn. (FC analysis groups: control (n=15), 0 hr (prior to breakdown, n=17), 12 hr (tissue breakdown, n=22), 24 hr (tissue repair, n=16) and 48 hr (tissue remodelling, n=10) after progesterone withdrawal; statistical comparisons were made using Kruskal-Wallis tests with multiple comparisons. * $p < 0.05$, ** $p < 0.01$, *** $p < 0.001$, **** $p < 0.0001$). **(J-K)** Immunohistochemical detection of $CD14^+$ monocytes (cyan), $CD64^+$ macrophages (yellow) and $Ly6G^+$ neutrophils (magenta) (merged and split channel) in uterine tissue cross sections at **(J)** 24 hr (repair, n=5) and **(K)** 48 hr (remodelling, n=3) following progesterone withdrawal (merged and split channel representative images, scale bar = 1000μm).

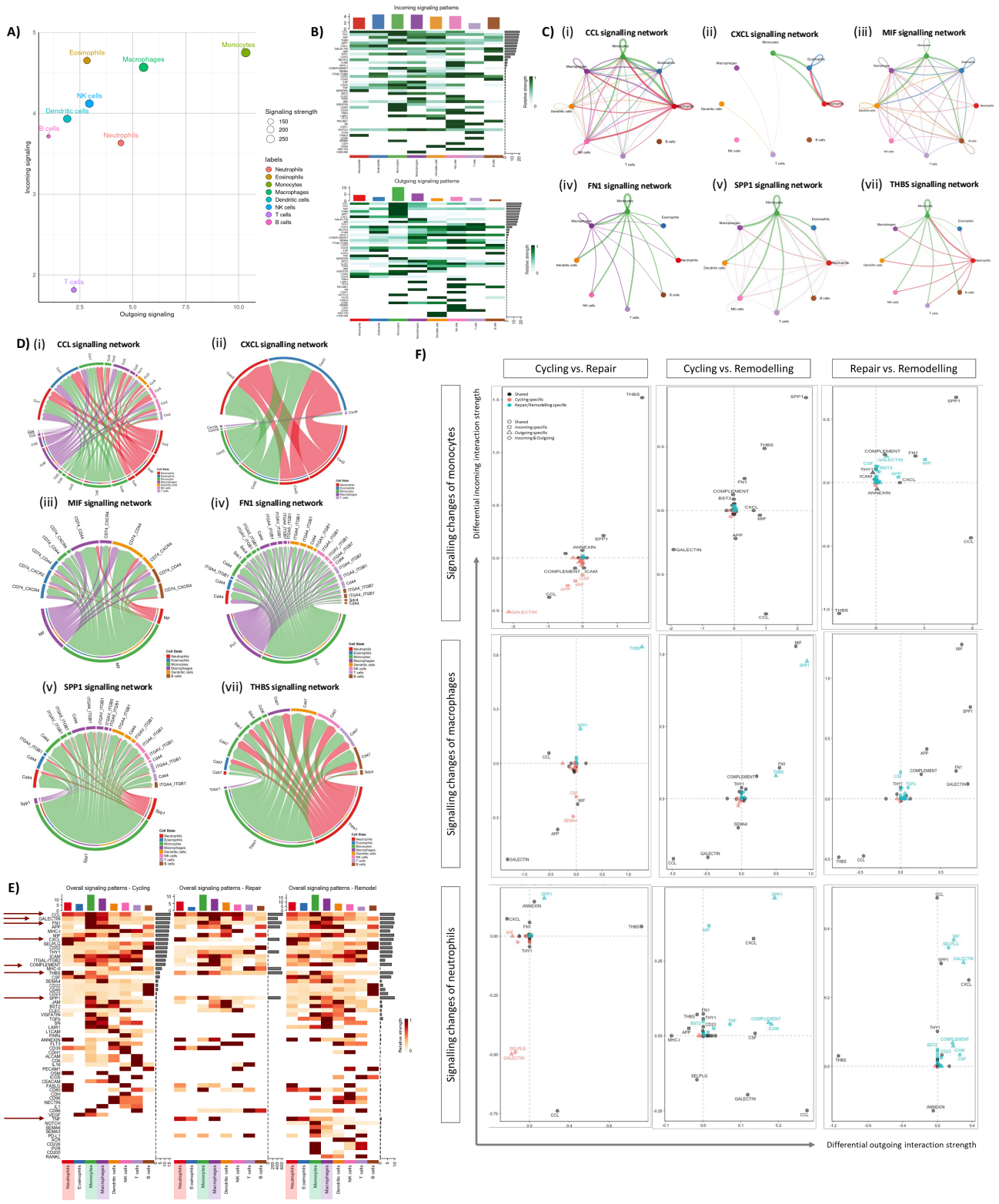


**Figure 5 – CellChat analysis of scRNAseq immune cell data infers intercellular communication networks associated with endometrial repair and remodelling. (A)**

801 Scatterplot: visualisation of overall signalling role of each cell group as determined by total
802 outgoing and incoming communication probability (dot size = total number of inferred links,
803 dot colour = different cell groups). **(B)** Heatmap: Outgoing and incoming signalling patterns
804 relative to cell type identifying top pathways in scRANseq data. **(C)** Circle plot: inter- and
805 intracellular communication networks between immune cell types for **(i)** CCL, **(ii)** CXCL, **(iii)**
806 MIF, **(iv)** FN1, **(v)** SPP1, **(vii)** THBS signalling pathways (circle size = number of cells in group,
807 connection width = probability of interaction). **(D)** Chord diagram: ligand-receptor pairs and
808 their weighted interactions between immune cells for **(i)** CCL, **(ii)** CXCL, **(iii)** MIF, **(iv)** FN1, **(v)**
809 SPP1, **(vii)** THBS signalling pathways (chord width = strength of interactions). **(E)** Heatmap:
810 Overall signalling patterns of immune cells relative to experimental condition, top 8 signalling
811 pathways highlighted with arrows (intensity of colour= relative signalling strength). **(F)**
812 Scatterplot: pairwise comparison of relative strength of signalling pathways in monocytes,
813 macrophages and neutrophils between experimental data set: cycling vs repair; cycling vs
814 remodelling; repair vs remodelling.

815

816 Supplementary data

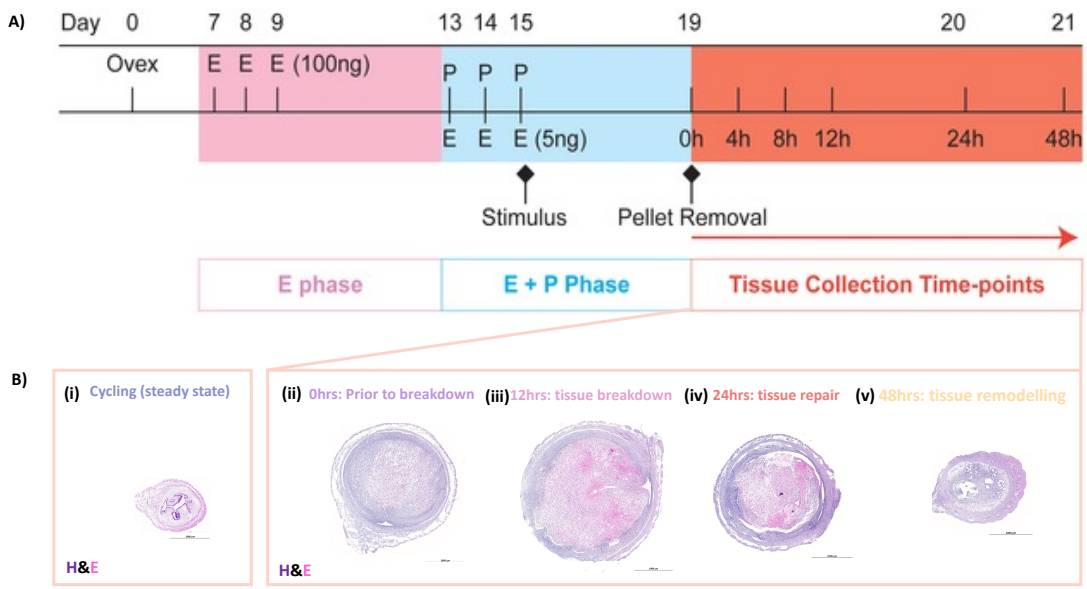


817

818 **Supplementary figure 1: Mouse model of simulated menstruation characterised by**
819 **endometrial tissue breakdown and repair. (A)** Schematic detailing the timeline of surgical
820 procedures and hormonal stimulation used to induce a menstruation-like event in mice. **(B)**
821 Haematoxylin and eosin (H&E) staining of uterine tissue sections demonstrate macro- and
822 microscopic tissue architecture in **(i)** steady state mouse uterus and mouse uterus at various
823 time points of tissue breakdown and repair: **(ii)** 0hrs, prior to breakdown; **(iii)** 12hrs, tissue
824 breakdown; **(iv)** 24hrs, endometrial repair; **(v)** 48hrs, endometrial remodelling (time post
825 progesterone withdrawal; scale bar=1000μm).

826

| Fluorophore | Antigen | Clone | Catalogue number | Dilution |
|---|---|---|---|---|
| BV421 | CD64 | X54-7/7.1 | 139309 | 1/100 |
| BV510 | CD45 | 30-F11 | 103138 | 1/200 |
| BV570 | CD3 | 17A2 | 100225 | 1/40 |
| BV785 | CD11c | N418 | 117335 | 1/100 |
| PE-Fire 640 | Ly6G | 1A8 | 127675 | 1/400 |
| PE/Dazzle 594 | Siglec F | E50-2440 | 562757 | 1/400 |
| PE/Cy7 | F4/80 | BM8 | 123114 | 1/200 |
| PerCP/Cy5.5 | Ly6C | HK1.4 | 128012 | 1/100 |
| AF700 | MHC II | M5/114.15.2 | 107622 | 1/200 |
| APC/Cy7 | CD11b | M1/70 | 101226 | 1/200 |
| Pacific blue | NK1.1 | PK136 | 108722 | 1/200 |
| Spark blue 550 | CD19 | 6D5 | 115565 | 1/200 |
| LIVE/DEAD Red | | | L34971 | 1 test per sample |

827

828 **Supplementary Table 1: Flow cytometry antibody panel utilised to characterise uterine**

829 **immune cell dynamics.**

A)

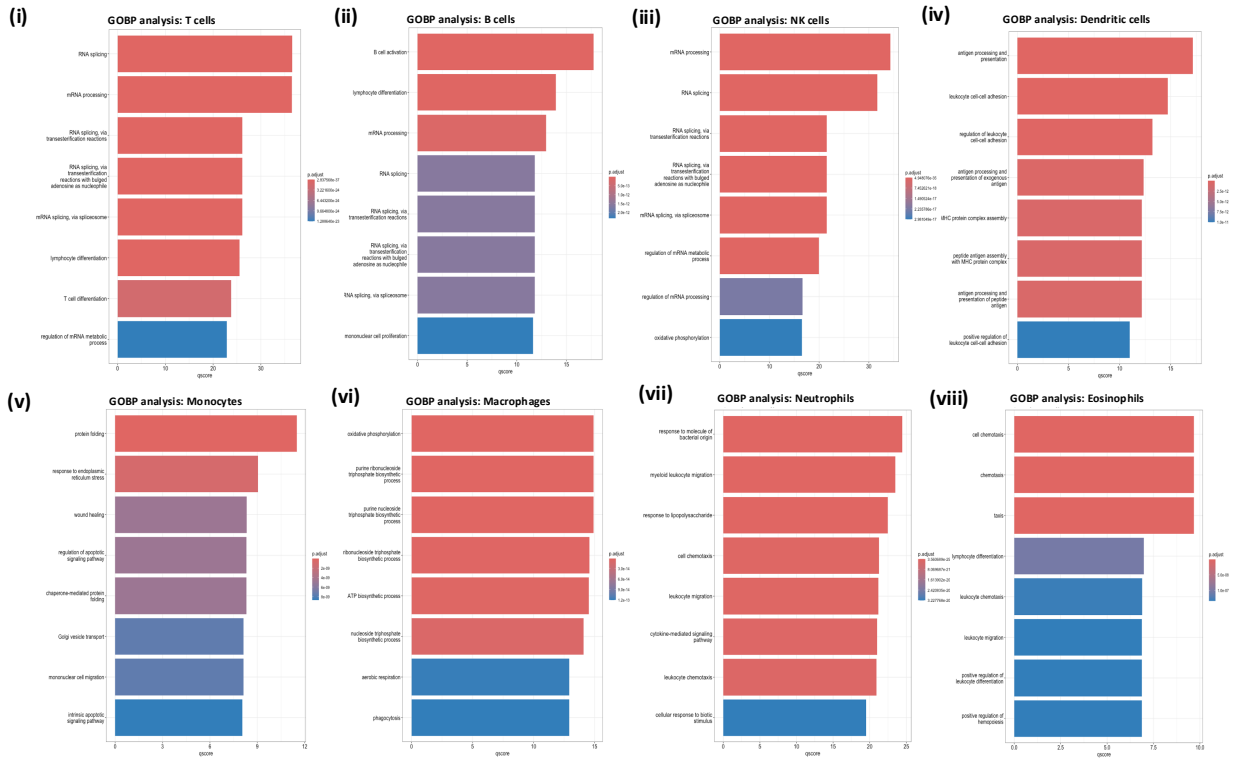
(i)
GOBP analysis: T cells
(ii)
GOBP analysis: B cells
(iii)
GOBP analysis: NK cells
(iv)
GOBP analysis: Dendritic cells
(v)
GOBP analysis: Monocytes
(vi)
GOBP analysis: Macrophages
(vii)
GOBP analysis: Neutrophils
(viii)
GOBP analysis: Eosinophils

B)

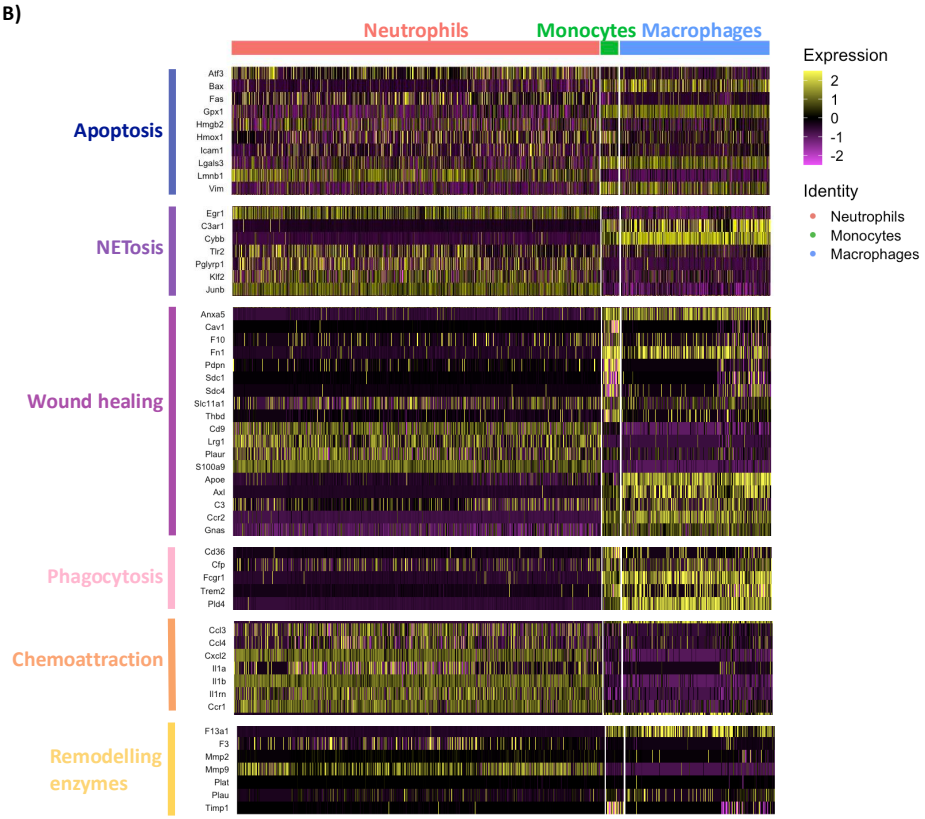
Neutrophils
Monocytes
Macrophages
Expression
2
1
0
-1
-2
Identity
Neutrophils
Monocytes
Macrophages
Apoptosis
Atf3
Bax
Fas
Gpx1
Hmgb2
Hmox1
Icam1
Lgals3
Lmnb1
Vim
NETosis
Egr1
C3ar1
Cybb
Tlr2
Pglyrp1
Klf2
Junb
Wound healing
Anxa5
Cav1
F10
Fn1
Pdpn
Sdc1
Sdc4
Slc11a1
Thbd
Cd9
Lrg1
Plaur
S100a9
Apoe
Axl
C3
Ccr2
Gnas
Phagocytosis
Cd36
Cfp
Fcgr1
Trem2
Pld4
Chemoattraction
Ccl3
Ccl4
Cxcl2
Il1a
Il1b
Il1rn
Ccr1
Remodelling enzymes
F13a1
F3
Mmp2
Mmp9
Plat
Plau
Timp1

832 **Supplementary figure 2: Gene Ontology (GO) analysis reveals biological processes**
833 **(BP) associated with the transcriptome of each immune cell cluster. (A)** Bar plot:
834 Unbiased analysis of GOBP terms associated with the genetic signature of each immune cell
835 cluster: **(i)** T cells **(ii)** B cells **(iii)** NK cells **(iv)** Dendritic cells **(v)** Monocytes **(vi)** Macrophages
836 **(vii)** Neutrophils **(viii)** Eosinophils. Bar size= qscore: -log(p.adjust) ; bar colour= P.adjust
837 value. **(B)** Heatmap (yellow, high; purple, low): Biased analysis of gene signatures (GSEA
838 gene sets) associated with known wound tissue repair GO terms by neutrophil, monocyte and
839 macrophage clusters: apoptosis, NETosis, wound healing, phagocytosis, chemoattraction,
840 remodelling enzymes. Top axis is colour coded and named by immune cell type.
841

842

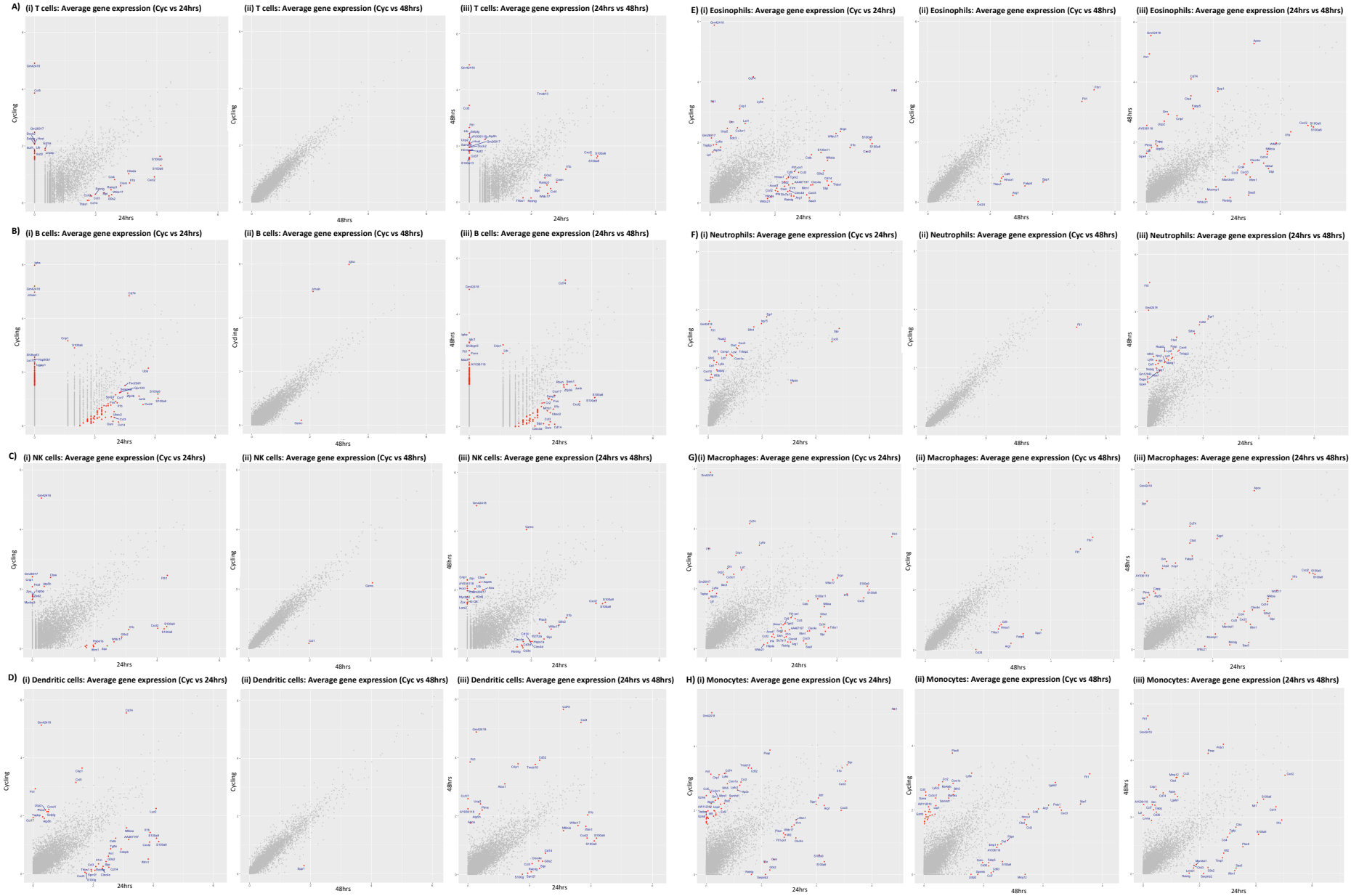
A) (i) T cells: Average gene expression (Cyc vs 24hrs)
(ii) T cells: Average gene expression (Cyc vs 48hrs)
(iii) T cells: Average gene expression (24hrs vs 48hrs)
E) (i) Eosinophils: Average gene expression (Cyc vs 24hrs)
(ii) Eosinophils: Average gene expression (Cyc vs 48hrs)
(iii) Eosinophils: Average gene expression (24hrs vs 48hrs)
B) (i) B cells: Average gene expression (Cyc vs 24hrs)
(ii) B cells: Average gene expression (Cyc vs 48hrs)
(iii) B cells: Average gene expression (24hrs vs 48hrs)
F) (i) Neutrophils: Average gene expression (Cyc vs 24hrs)
(ii) Neutrophils: Average gene expression (Cyc vs 48hrs)
(iii) Neutrophils: Average gene expression (24hrs vs 48hrs)
C) (i) NK cells: Average gene expression (Cyc vs 24hrs)
(ii) NK cells: Average gene expression (Cyc vs 48hrs)
(iii) NK cells: Average gene expression (24hrs vs 48hrs)
G)(i) Macrophages: Average gene expression (Cyc vs 24hrs)
(ii) Macrophages: Average gene expression (Cyc vs 48hrs)
(iii) Macrophages: Average gene expression (24hrs vs 48hrs)
D) (i) Dendritic cells: Average gene expression (Cyc vs 24hrs)
(ii) Dendritic cells: Average gene expression (Cyc vs 48hrs)
(iii) Dendritic cells: Average gene expression (24hrs vs 48hrs)
H) (i) Monocytes: Average gene expression (Cyc vs 24hrs)
(ii) Monocytes: Average gene expression (Cyc vs 48hrs)
(iii) Monocytes: Average gene expression (24hrs vs 48hrs)
Cycling
24hrs
48hrs

843 **Supplementary figure 3: Average gene expression analysis for each immune cell**
844 **cluster between the 3 experimental conditions.** Scatter plot: Average gene expression
845 analysis for each immune cell cluster **(A)** T cells **(B)** B cells **(C)** NK cells **(D)** Dendritic cells **(E)**
846 Monocytes **(F)** Macrophages **(G)** Neutrophils **(H)** Eosinophils between different experimental
847 conditions: **(i)** Cycling vs 24 hr **(ii)** Cycling vs 48 hr **(iii)** 24 hr vs 48 hr.
848

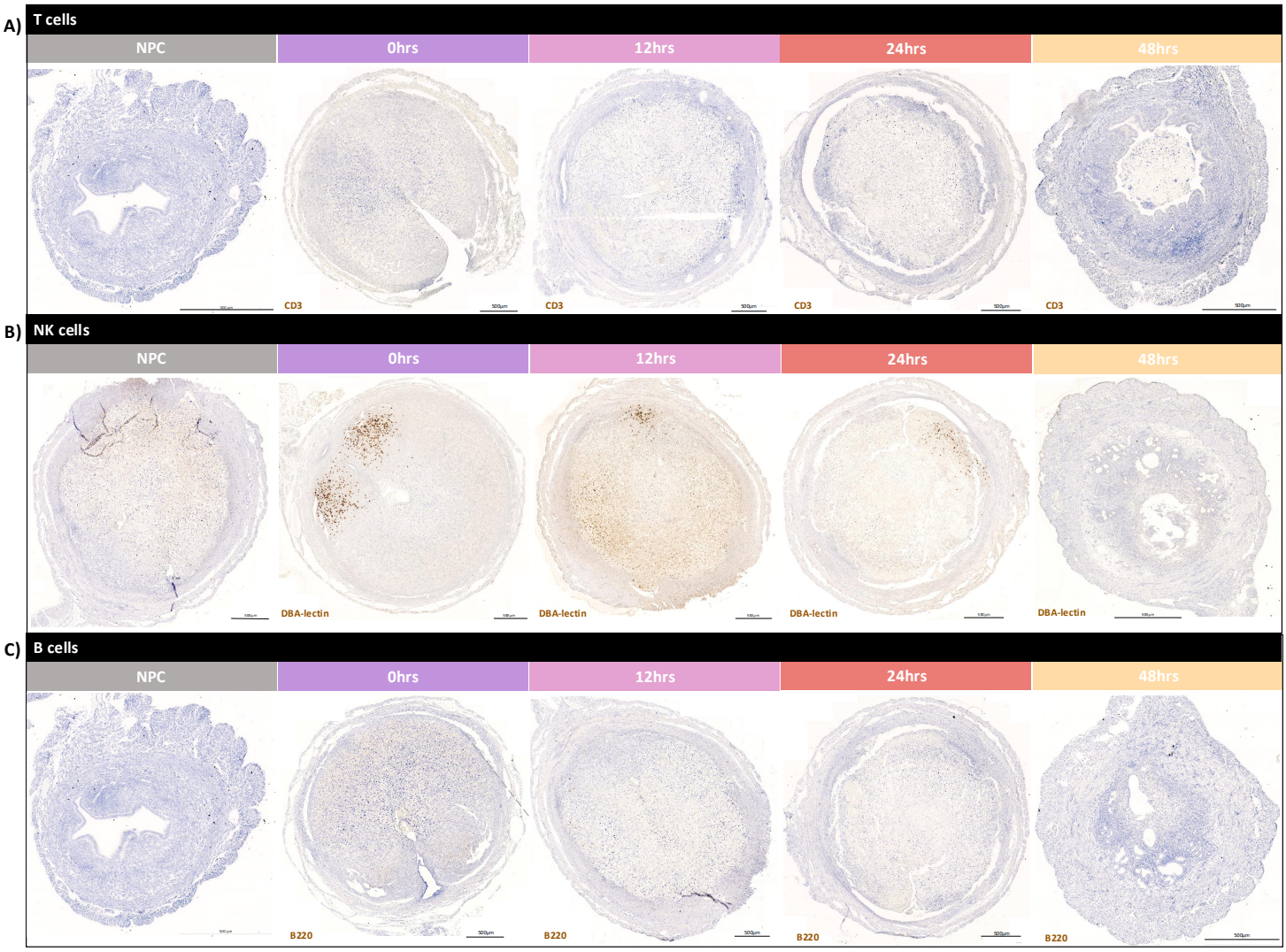


**Supplementary figure 4: Immunohistochemistry analysis of uterine lymphocyte dynamics during endometrial repair using a mouse model of simulated menstruation.** Immunohistochemistry: detection of **(A)** CD3+ T cells, **(B)** DBA-lectin+ NK cells and **(C)** B220+ B cells in uterine tissue sections at 0hr (prior to breakdown, n=4), 12hr (tissue breakdown, n=4-6), 24hr (tissue repair, n=4-5) and 48hr (tissue remodelling, n=4-6) hr after progesterone withdrawal (representative images, scale bar=500μm).

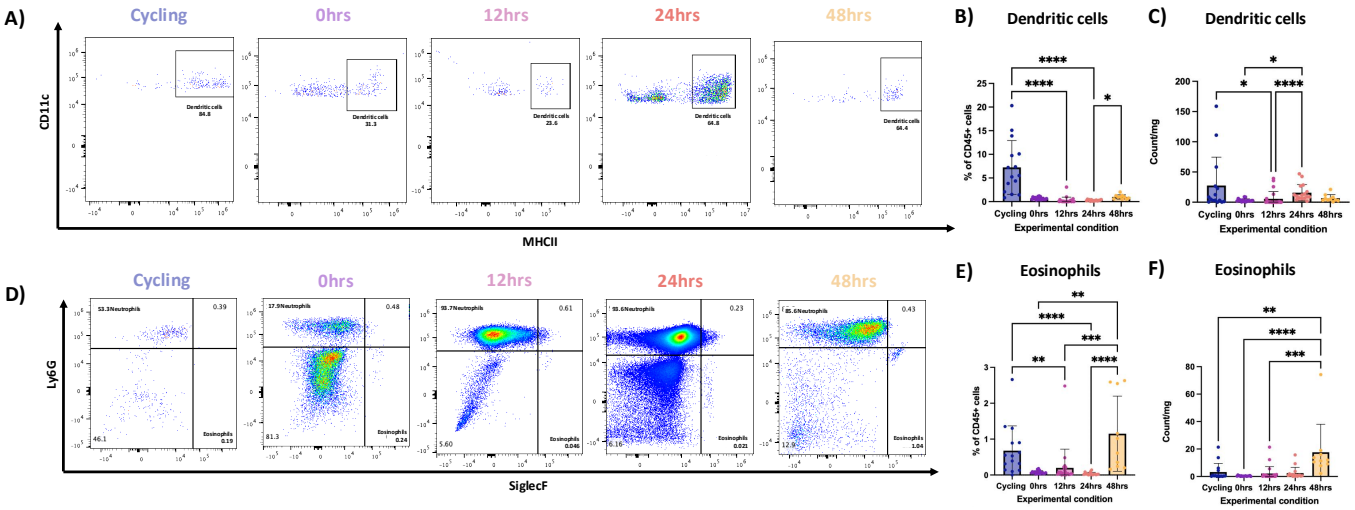


**Supplementary figure 5: Flow cytometry analysis of dendritic cells and eosinophils in uterine tissues endometrial repair using a mouse model of simulated menstruation. (A)** Population restricted FC analysis to identify CD45+ CD3- CD19- NK1.1- Ly6G- CD64- CD11c+ MHCII+ dendritic cells (DCs) in uterine tissue digests. **(B)** Bar plot, FC quantification: Relative abundance of DCs calculated as a percentage of total CD45+ cells per uterine horn. **(C)** Bar plot, FC quantification: Absolute counts of DCs per uterine horn. **(D)** Population restricted FC analysis to CD45+ CD3- CD19- NK1.1- CD11b+ Ly6G- SiglecF+ eosinophils in uterine tissue digests. **(E)** Bar plot, FC quantification: Relative abundance of eosinophils calculated as a percentage of total CD45+ cells per uterine horn. **(F)** Bar plot, FC quantification: Absolute counts of eosinophils per uterine horn. (FC analysis groups: control (n=15), 0hr (prior to breakdown, n=17), 12hr (tissue breakdown, n=22), 24hr (tissue repair, n=16) and 48hr (tissue remodelling, n=10) after progesterone withdrawal; statistical comparisons were made using Kruskal-Wallis tests with multiple comparisons. and * $p < 0.05$, ** $p < 0.01$, *** $p < 0.001$, **** $p < 0.0001$).

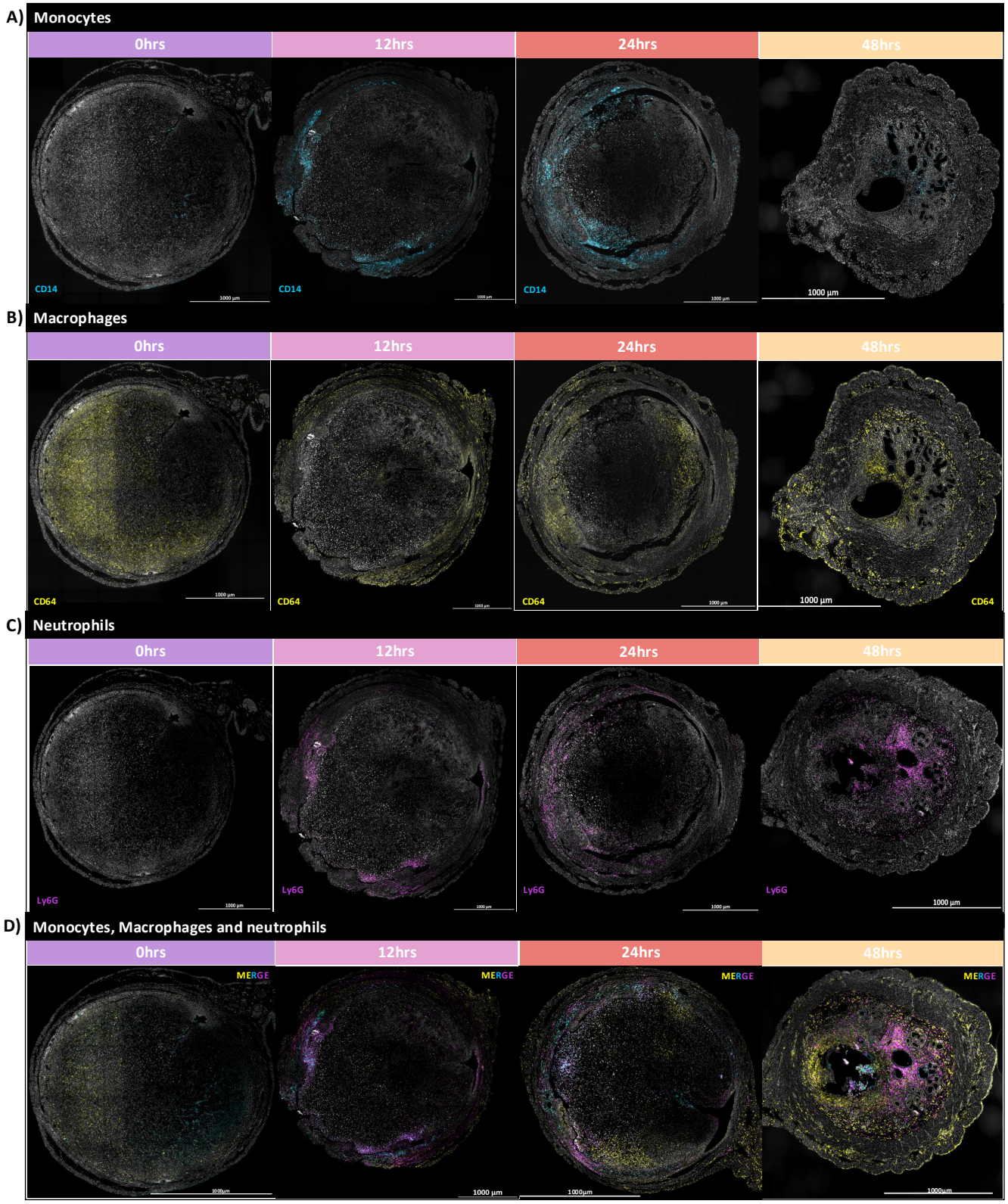


873

874 **Supplementary figure 6: Immunohistochemistry analysis of myeloid cell dynamics**
875 **during endometrial repair using a mouse model of simulated menstruation.**
876 Immunohistochemical detection of **(A)** CD14+ monocytes (cyan), **(B)** CD64+ macrophages
877 (yellow) and **(C)** Ly6G+ neutrophils (magenta) in uterine tissue sections at 0hr (prior to

878 breakdown, n=4), 12hr (tissue breakdown, n=5), 24hr (tissue repair, n=5) and 48hr (tissue
879 remodelling, n=3) following progesterone withdrawal (representative images, scale
880 bar=1000μm). (D) Merged channel representative images (scale bar=1000μm).
881

882 **Appendix**

883 Abbreviations

| Abbreviation | Full term |
|---|---|
| Acod1 | Aconitate decarboxylase 1 |
| Adgre1 | Adhesion G protein–coupled receptor E1 (F4/80) |
| Anxa5 | Annexin A5 |
| Apoe | Apolipoprotein E |
| APP | Amyloid precursor protein |
| AWERB | Animal Welfare and Ethical Review Body |
| Axl | AXL receptor tyrosine kinase |
| Cav1 | Caveolin 1 |
| C3 | Complement component 3 |
| Ccl2 | C–C motif chemokine ligand 2 |
| Ccl3 | C–C motif chemokine ligand 3 |
| Ccl4 | C–C motif chemokine ligand 4 |
| Ccl5 | C–C motif chemokine ligand 5 |
| Ccl6 | C–C motif chemokine ligand 6 |
| Ccl9 | C–C motif chemokine ligand 9 |
| CCL | C–C motif chemokine ligand |
| CCR2 | C–C motif chemokine receptor 2 |
| Cd3e | CD3 epsilon chain |
| CD3 | Cluster of differentiation 3 |
| CD9 | Cluster of differentiation 9 |
| CD11b | Integrin alpha M |
| CD11c | Integrin alpha X |
| CD14 | Cluster of differentiation 14 |
| CD19 | Cluster of differentiation 19 |
| CD45 | Protein tyrosine phosphatase receptor type C |
| CD64 | Fc gamma receptor I |
| Cd68 | Cluster of differentiation 68 |
| Cdc1 | Conventional dendritic cell 1 |
| cDNA | Complementary DNA |
| Clec9a | C-type lectin domain family 9 member A |
| Clec10 | C-type lectin domain family 10 |
| Csf1r | Colony stimulating factor 1 receptor |
| CXCL | C-X-C motif chemokine ligand |
| Cxcl1 | C-X-C motif chemokine ligand 1 |
| Cxcl3 | C-X-C motif chemokine ligand 3 |
| Cxcr2 | C-X-C motif chemokine receptor 2 |
| CXCL8 | C-X-C motif chemokine ligand 8 |
| DCs | Dendritic cells |
| DEGs | Differentially expressed genes |
| Dusp1 | Dual specificity phosphatase 1 |
| E2 | Estradiol |
| EDTA | Ethylenediaminetetraacetic acid |

| Abbreviation | Full term |
|---|---|
| F10 | Coagulation factor X |
| F4/80 | Macrophage marker (Adgre1) |
| FACS | Fluorescence-activated cell sorting |
| FC | Flow cytometry |
| FFPE | Formalin-fixed paraffin-embedded |
| FN1 | Fibronectin 1 |
| Fn1 | Fibronectin 1 |
| FSC-A | Forward scatter area |
| FSC-H | Forward scatter height |
| GEMs | Gel bead-in-Emulsions |
| GO | Gene ontology |
| GOBP | Gene ontology biological processes |
| Gata3 | GATA binding protein 3 |
| Gnas | GNAS complex locus |
| Gzmb | Granzyme B |
| H2-Ab1 | MHC class II antigen A, beta 1 |
| Hic1 | Hypermethylated in cancer 1 |
| HMB | Human menopausal blood |
| HRP | Horseradish peroxidase |
| Ighd | Immunoglobulin heavy constant delta |
| IL-1β | Interleukin 1 beta |
| IL-6 | Interleukin 6 |
| Inha | Inhibin alpha |
| ISG15 | Interferon-stimulated gene 15 |
| IFIT1 | Interferon-induced protein with tetratricopeptide repeats 1 |
| IFIT3 | Interferon-induced protein with tetratricopeptide repeats 3 |
| Klrb1c | Killer cell lectin-like receptor B1C |
| Lrg1 | Leucine-rich alpha-2-glycoprotein 1 |
| Ly6C | Lymphocyte antigen 6 complex, locus C |
| Ly6G | Lymphocyte antigen 6 complex, locus G |
| MAPK | Mitogen-activated protein kinase |
| Mertk | MER proto-oncogene tyrosine kinase |
| MHC II | Major histocompatibility complex class II |
| MIF | Macrophage migration inhibitory factor |
| MMP | Matrix metalloproteinase |
| Msr1 | Macrophage scavenger receptor 1 |
| NET | Neutrophil extracellular trap |
| NK1.1 | Natural killer cell marker |
| Ncr1 | Natural cytotoxicity triggering receptor 1 |
| P4 | Progesterone |
| PCA | Principal component analysis |
| Pdpn | Podoplanin |
| PBS | Phosphate-buffered saline |
| Plaur | Plasminogen activator, urokinase receptor |
| QC | Quality control |

| Abbreviation | Full term |
|---|---|
| RNA | Ribonucleic acid |
| Rsad2 | Radical S-adenosyl methionine domain containing 2 |
| S100a8 | S100 calcium-binding protein A8 |
| S100a9 | S100 calcium-binding protein A9 |
| ScRNAseq | Single-cell RNA sequencing |
| Sdc1 | Syndecan 1 |
| Sdc4 | Syndecan 4 |
| Sell | L-selectin |
| SiglecF | Sialic acid-binding Ig-like lectin F |
| Slc11a1 | Solute carrier family 11 member 1 |
| SPP1 | Secreted phosphoprotein 1 |
| SSC-A | Side scatter area |
| SSC-H | Side scatter height |
| TGF-β | Transforming growth factor beta |
| TGFBI | Transforming growth factor beta-induced |
| THBS1 | Thrombospondin 1 |
| Thbd | Thrombomodulin |
| Tmem123 | Transmembrane protein 123 |
| TNF-α | Tumour necrosis factor alpha |
| TPM | Transcripts per million |
| TSP-1 | Thrombospondin-1 |
| UMAP | Uniform Manifold Approximation and Projection |
| uNKs | Uterine natural killer cells |
| VEGF | Vascular endothelial growth factor |
| Xcr1 | X-C motif chemokine receptor 1 |

884